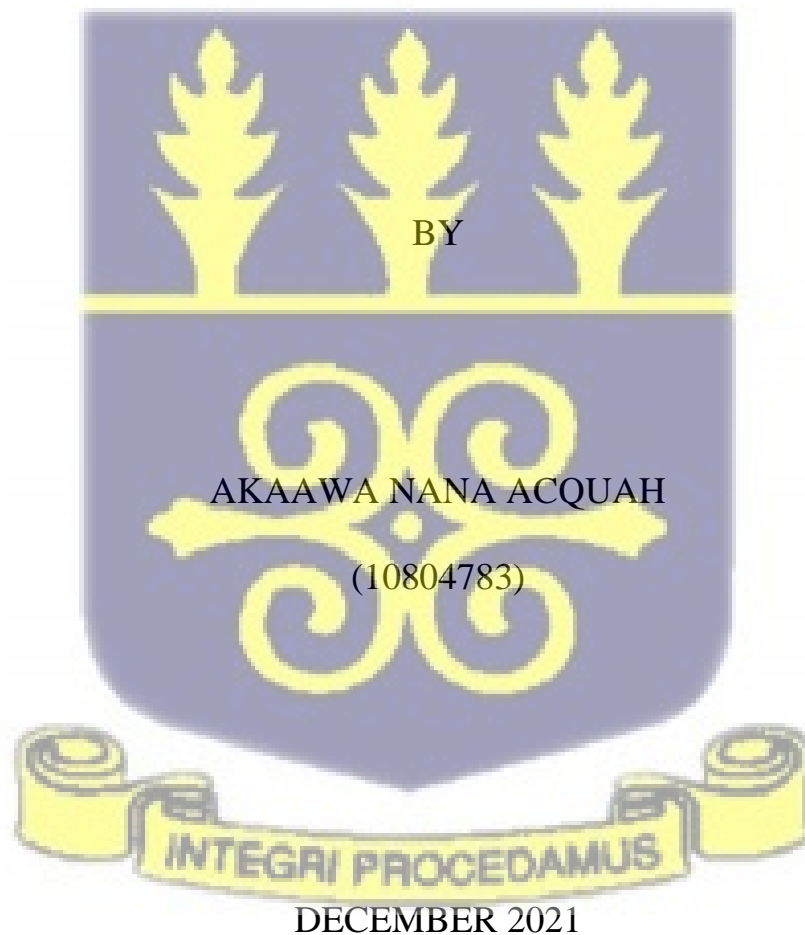


**DOSIMETRIC STUDY OF IMAGE-GUIDED BRACHYTHERAPY  
FOR CERVIX CARCINOMA TREATMENT AT KOMFO ANOKYE  
TEACHING HOSPITAL**

This thesis/dissertation is to be submitted to the University of Ghana - Legon in partial fulfillment of the requirement for the award of MPhil Medical Physics Degree.



## DECLARATION

This dissertation is the outcome of a research done by Akaawa Nana Acquah in the Department of Medical Physics, School of Nuclear and Allied Sciences (SNAS), University of Ghana-Legon, under the supervision of Mr. Eric Kotei Addison (KATH, KNUST), Dr. Francis Hasford (HOD-SNAS, GEAC) and Prof. Anne Beate L. Marthinsen (NTNU-Norway). I affirm that, no part of this work has been presented in part or whole to any other university or institution for the award of a diploma or degree at any level. Accordingly other works and/or researches done by other researches cited in this work have been acknowledged under references.

Sign   
Akaawa Nana Acquah  
(Student)

Date ---15/12/2021-----

Sign   
Dr. Francis Hasford  
(Co - Supervisor)

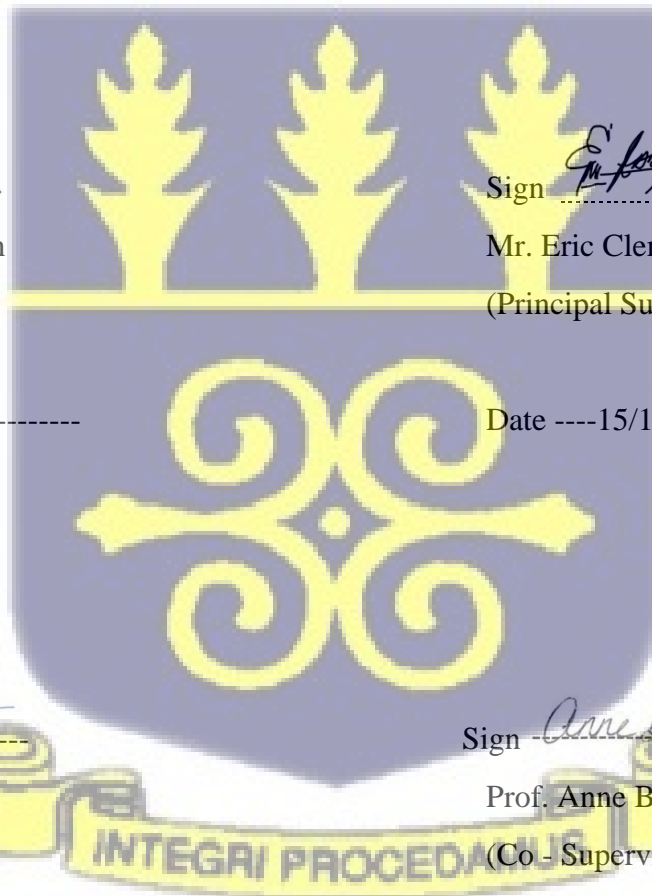
Date ---15/12/2021-----

Sign   
Mr. Eric Clement Desmond Kotei Addison  
(Principal Supervisor)

Date ---15/12/2021-----

Sign   
Prof. Anne Beate L. Marthinsen  
(Co - Supervisor)

Date ---15/12/2021-----



## ABSTRACT

The study was conducted purposely to compare the dosimetric characteristics of 2D to 3D LDR; to compare their planning procedures, imaging, and dose distributions in both treatment modalities to provide recommendations for an easy transition from 2D LDR to 3D IGBT at KATH. The lack of spatial information on the tumour and OAR volumes and the inability to visualize the extent of the tumour and applicators in 3D results in suboptimal application technique planning with insufficient dose coverage for large tumours, which is a major limitation of brachytherapy treatment planning at KATH. Perspex and water were used in the construction of a water phantom for data collection of certain parameters such as air kerma strength of the sources and dose distribution across the phantom. Both 2D and 3D imaging modalities, X-ray and CT, were utilized and compared, including treatment planning procedures, to develop measurable data on the differences, advantages, and demerits of 2D LDR and 3D IGBT. To determine dosage distribution, cross-calibration measurement was performed to get the correction factor for the ion chamber used for the data collection, which was unavailable. The values obtained for  $K_{Q0}$ ,  $K_{T,P}$ ,  $K_{POL}$ ,  $K_{SAT}$  for cobalt were 8.892, 1.030, 0.975, and 8.854, respectively and the correction factor ( $D_A, Q$ ) for PTW 31010 was  $3.240 \pm 0.06 \times 10^6$  Gy/C. Furthermore, the dose distribution in 2D is point-based and hence volumetric dose distribution is not considered as done in 3D format, which implies that there may be doses beyond the 2 cm margin which are not accounted for during the treatment planning. This and poor imaging in 2D to visualize the crossing of the urethra artery and ureter verifies that point A is not a necessity in 3D LDR IGBT. 2D LDR may have come with some benefits. With the successful construction of the phantom, collection, and analysis of dosimetric parameters, it can be concluded that Image-guided brachytherapy is observed to be quite advantageous in a radioactive source and organ localization, treatment planning, safety, and even cost.

## **DEDICATION**

This study is dedicated to my parents Mr. Solomon Ato Acquah and Mrs. Gloria Acquah for their emotional, mental and financial support as well as prayers throughout my education and the period of this study. I really appreciate all their effort. I hope that they would appreciate Medical Physics some more because of this work done.



## ACKNOWLEDGEMENTS

There are many people I would like to acknowledge as I have received help and support from many but to commence, I would like to give gratitude to the Lord God Almighty. I had life and strength to go through all of this because of His grace. To Mr. Eric K. T. Addison, Dr. Francis Hasford and Professor Anne Beate L. Marthinsen who have been the best supervisors, I would like to acknowledge for the financial and physical support and guidance. This study wouldn't have been a possibility without them. The staff of KATH Oncology – Medical Physics Department, especially Mr. Kingsley Akosah, helped me a during my data collection, thus, I would like to appreciate them for everything. My gratitude goes to the School of Nuclear and Allied Sciences and all lecturers of the Medical Physics Department for their guidance throughout the period of the study. Lastly, I want to appreciate all family and friends (Mercy Torshie Schandorf) for being there throughout this period and for their support. Thanks to all.

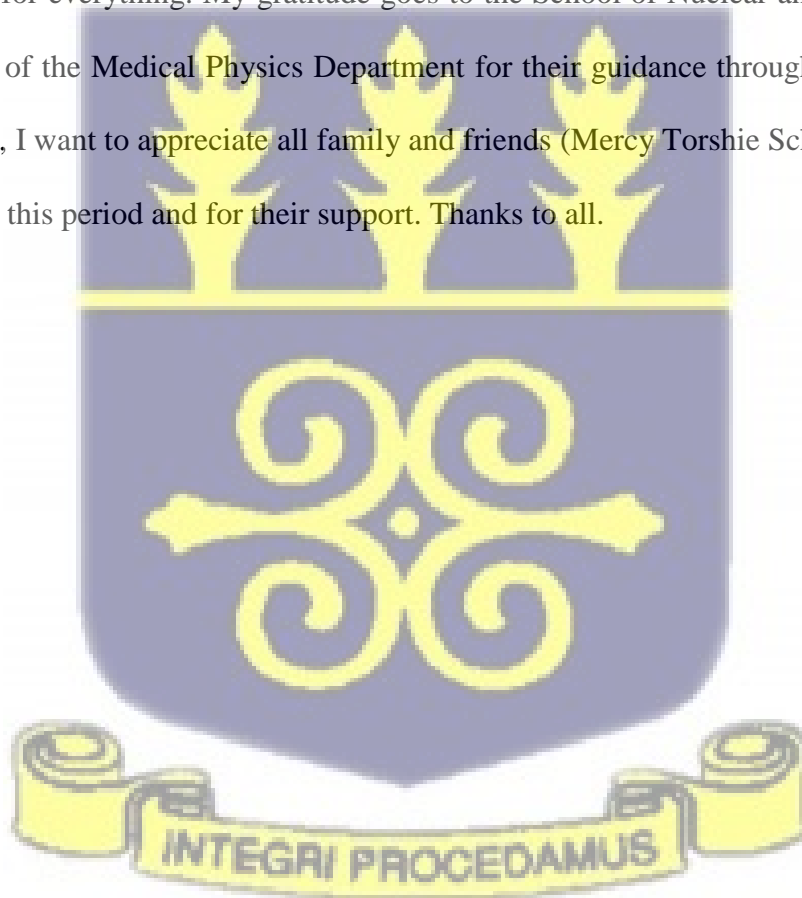


## TABLE OF CONTENTS

DECLARATION.....	ii
ABSTRACT.....	iii
DEDICATION.....	iv
ACKNOWLEDGEMENTS .....	v
LIST OF FIGURES.....	viii
LIST OF TABLES.....	ix
ABBREVIATIONS.....	x
<b>1.0 INTRODUCTION.....</b>	<b>1</b>
1.1 <i>Background</i> .....	1
1.2 <i>Problem statement</i> .....	2
1.3 <i>Relevance and justification</i> .....	3
1.4 <i>Scope of the study</i> .....	4
1.5 <i>Objectives of Study</i> .....	4
<b>CHAPTER TWO .....</b>	<b>8</b>
<b>2.0 LITERATURE REVIEW.....</b>	<b>8</b>
2.1 <i>Clinical Outcomes from IGABT studies</i> .....	8
2.2 <i>Target volumes, Dose and OARs</i> .....	9
2.3 <i>IMRT versus IGABT</i> .....	11
2.4 <i>Point A consideration</i> .....	13
2.5 <i>2D LDR versus 3D HDR (cost)</i> .....	16
2.6 <i>Imaging modalities for IGABT</i> .....	17
2.7 <i>Dose specification</i> .....	22
<b>CHAPTER THREE.....</b>	<b>26</b>
<b>3.0 METHODOLOGY .....</b>	<b>26</b>
3.1 <i>Materials</i> .....	26
3.1.1 <i>Ionization chamber</i> .....	28
3.1.2 <i>Types of sources</i> .....	29
3.1.3 <i>Imaging</i> .....	30
3.1.4 <i>Applicator system</i> .....	31
3.2 <i>Methods</i> .....	32
3.2.1 <i>Phantom Design</i> .....	32
3.2.2 <i>Treatment planning</i> .....	33

3.2.3	<i>Data Collection</i> .....	34
<b>CHAPTER FOUR</b> .....		35
4.0	<b>RESULTS AND DISCUSSION</b> .....	35
4.1	<i>Comparison of 2D&amp;3D Imaging</i> .....	35
4.2	<i>Comparison of 2D&amp;3D planning</i> .....	36
4.3	<i>Dosimetry</i> .....	38
4.4	<i>Limitations</i> .....	40
4.5	<i>Recommendations</i> .....	40
<b>CHAPTER FIVE</b> .....		41
5.0	<b>CONCLUSION</b> .....	41
7.0	<b>Appendix 1: Air Kerma Strength</b> .....	50
7.1	<b>Appendix 2: Dose distribution in water phantom</b> .....	53
7.1	<b>Appendix 3: Cross calibration</b> .....	54



## LIST OF FIGURES

Figure 1. Side view of constructed jig with dimensions in the Perspex water phantom container. .....	32
Figure 2. Block diagram of the jig used to hold the applicators in place in the water phantom... 32	32
Figure 3. Image of moulded gelatin.....	26
Figure 4. Image of gelatin 9 hours after moulding in room temperature.....	26
Figure 5. Image of prototype of jig for water phantom made with wood.....	28
Figure 6. Image of perspex of jig for water phantom used to hold applicators. ....	28
Figure 7. Image of calibrated ionization chamber in water phantom during taking data collection .....	29
Figure 8. CT image taken prototype of the water phantom jig with tandem and ovoids in a water. .....	31
Figure 9. A diagram illustrating the geometric points A and B.....	23
Figure 10. Modern style adjustable Manchester style fletcher applicator showing the tandem and ovoids.....	31
Figure 11. An implant patient's AP (planes a) and lateral (planes b) views are depicted in a schematic diagram of a 60-Gy dose. The width, length, and thickness of the 60-Gy dose isodose volumes are measured while accounting for external dose contribution.....	15
Figure 12. Treatment chain for image-guided adaptive cervix cancer brachytherapy. ....	<b>Error!</b>
<b>Bookmark not defined.</b>	
Figure 13. A slice from CT imaging of a water phantom with metallic applicators showing artifacts.....	35

Figure 14. X-ray images of lateral and anterior view of applicators in water phantom respectively.  
 ..... 36

Figure 15. Image of DVH showing dose distribution to the various organ volumes. .... 37

Figure 16. Graph of distance against air kerma strength  $S_k$  ( $Gycm^2h^{-1}$ ) x  $10^{-12}$  ..... **Error!**

**Bookmark not defined.**

Figure 17. A graph of dose distribution in the water phantom showing the relation between dose and distance..... 39



**LIST OF TABLES**

Table 1. Imaging modalities in cervix carcinoma and their effects on brachytherapy planning. . 18

Table 2. A table of showing dose delivered and during 3D treatment planning ..... 37

Table 3. Charge, exposure rates and air kerma strength values of air kerma strength of sources V1, U3 and V5. .... 50

Table 4. Charge values of dose distribution with varying distances at the right side of the source.  
 ..... 53

Table 5. Charge values of radiation quantity at a depth of 10 cm in phantom. .... 54

Table 6. Charge values of ionization recombination measurement at a depth of 10 cm in phantom.  
 ..... 55

Table 7. Charge values of ionization recombination measurement at a depth of 10 cm in phantom.  
 ..... 56

Table 8. Charge values of ionization recombination measurement at a depth of 10 cm in phantom.  
..... 57

Table 9. Parameters for correction factor calculation for cross calibration..... 60

## ABBREVIATIONS

2D: Two dimensional

3D: Three dimensional

4D: Four Dimensional

2D-HDR-BT: Two Dimensional High Dose Rate Brachytherapy

2D LDR: Two Dimensional Low Dose Rate

2D-LDR-BT: Two Dimensional Low Dose Rate Brachytherapy

3D BT: Three Dimensional Brachytherapy

3D CRT: Three Dimensional Conformal Radiotherapy

3D EBRT: Three Dimensional External Beam Radiotherapy

3D-HDR-BT: Three Dimensional High Dose Rate Brachytherapy

3D LDR BT: Three Dimensional Low Dose Rate Brachytherapy

IIA: Stage 2A

IB: Stage 1B

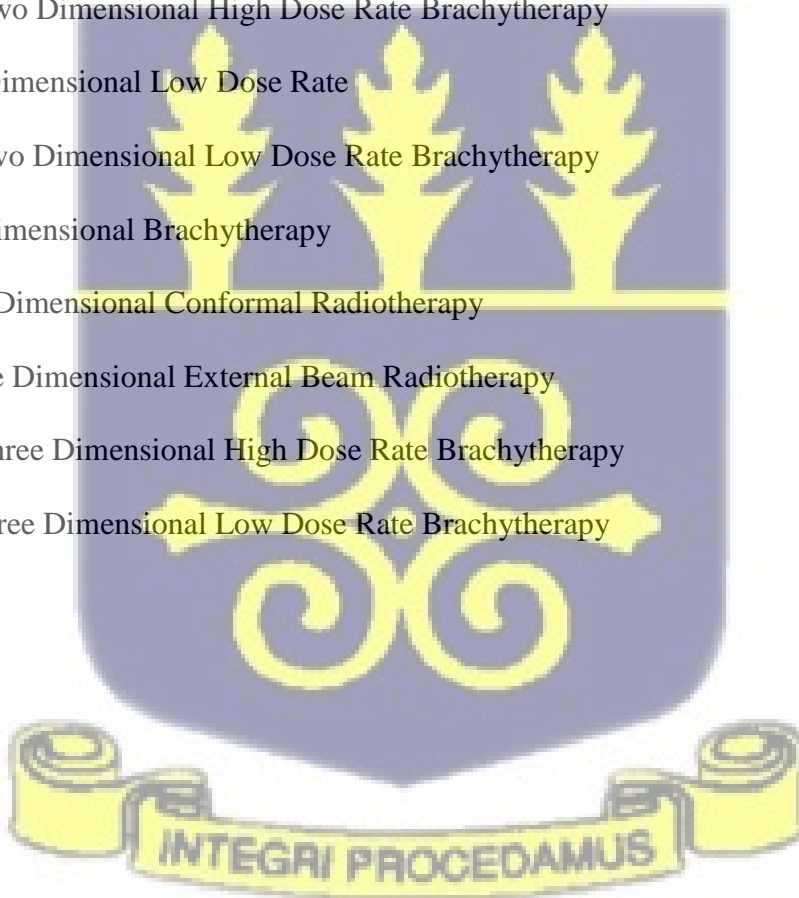
IIB: Stage 2B

IIIB: Stage 3B

IVA: Stage 4A

AP: Anterior-Posterior

BEV: Beam Eye View



BT: Brachytherapy

CT: Computed Tomography

CTV<sub>IR</sub>: Clinical Target Volume (Intermediate Risk)

CTV<sub>HR</sub>: Clinical Target Volume (High Risk)

D<sub>90</sub>: the dose that covers 90% of the target volume

D<sub>98</sub>: the dose that covers 98% of the target volume

DCE-MRI: Dynamic Contrast-Enhanced Magnetic Resonance Imaging

DEXA: Dual X-ray Absorptiometry

DW: Dose – Water

DW-MRI: Diffusion Weighted Magnetic Resonance Imaging

DV: Dose-Volume

DVH: Dose Volume Histogram

EBRT: External Beam Radiotherapy

EMBRACE: Image Guided Intensity Modulated External Beam Radiochemotherapy and MRI based adaptive Brachytherapy in locally advanced Cervical Cancer.

FDG-PET: Flurodeoxyglucose Positron Emission Tomography

FIGO: The International Federation of Gynecology and Obstetrics

G1: Grade 1 (well differentiated – low grade)

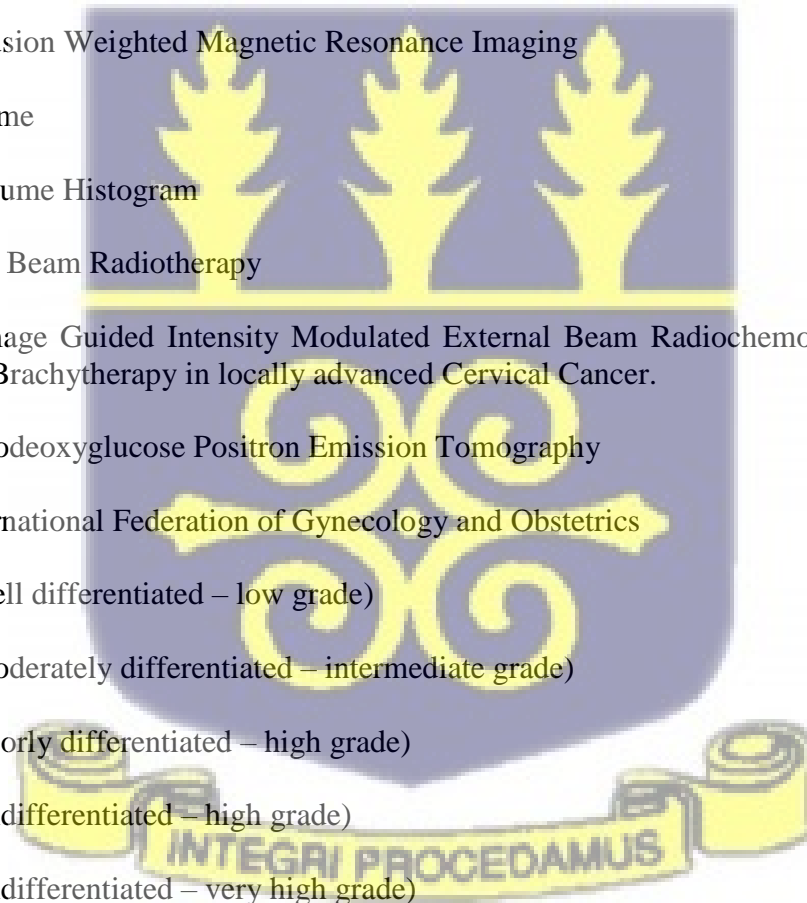
G2: Grade 2 (moderately differentiated – intermediate grade)

G3: Grade 3 (poorly differentiated – high grade)

G4: Grade 4 (undifferentiated – high grade)

G5: Grade 5 (undifferentiated – very high grade)

GEC-ESTRO GYN: The Groupe European de Curietherapie and European Society for Radiotherapy & Oncology Gyneacology.



GTV: Gross Tumour Volume

GTVres: Gross Tumour Volume

HDR: High Dose Rate

IC: Intra-cavitary

ICRU: International Commission on Radiation Units and Measurements

IGABT: Image Guided Adaptive Brachytherapy

IGBT: Image-guided brachytherapy

IGRT: Image Guided Radiotherapy

IMRI: Intraoperative Magnetic Resonance Imaging

IS: Interstitial

KATH: Komfo Anokye Teaching Hospital

$K_{Q,Q_0}$ : correction factor for beam quality

$K_{T,P}$ : correction factor for air density

$K_{POL}$ : correction factor for polarity effects

$K_{SAT}$ : correction factor for missing saturation

LDR: Low Dose Rate

MD: Medical Doctor

MRI: Magnetic Resonance Imaging

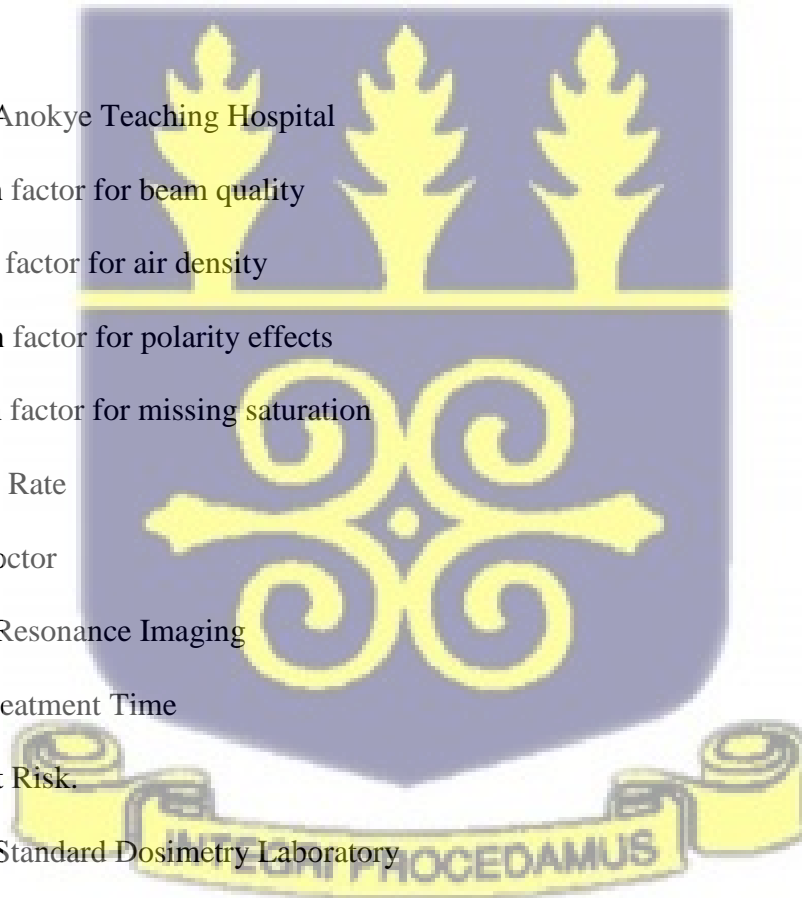
OTT: Overall Treatment Time

OAR: Organs At Risk.

PSDL: Primary Standard Dosimetry Laboratory

PTV: Planning Target Volume

RetroEMBRACE: Retrospective Image Guided Intensity Modulated External Beam Radiochemotherapy and MRI based adaptive Brachytherapy in locally advanced Cervical Cancer.



TLD: Thermoluminiscent Dosimeter

TPS: Treatment Planning System

VMAT: Volumetric Modulated Arc Therapy

WHO: World Health Organization



## **CHAPTER ONE**

### **1.0 INTRODUCTION**

#### **1.1 *Background***

Three-dimensional (3D) planning for external beam radiotherapy (EBRT) was a major achievement for more individualized patient treatment, better clinical outcomes, and reduced toxicity <sup>(1)</sup>. Brachytherapy, however, is still mostly based on 2D treatment planning in some radiotherapy centers in Ghana. The transition to 3D image-guided brachytherapy planning for most common brachytherapy indications, such as cervical cancers, is a logical development. Clinical brachytherapy involves inserting an applicator close to or into a targeted tumour (site) in which radioactive sources (<sup>192</sup>Ir, <sup>137</sup>Cs, <sup>60</sup>Co) can be inserted or placed in close proximity to the tumour. The applicator placement is done by a radiation oncology technician. These sources could either have a high or a low dose rate. Gynaecological cancer is the second commonest diagnosed female disease and is more prevalent in developing countries <sup>(2)</sup>. Besides that, it ranks as a common type of cancer in Ghanaian women between the ages of 15 and 44 years. As per current estimates, 3,052 women are identified with cervix carcinoma every year and 1,556 women's deaths are recorded from this disease <sup>(3)</sup>. The treatment option for cervical carcinoma is determined by its stage, the size, and histology of the tumour, the likelihood of lymph node involvement, and the patient's age and physical condition <sup>(2)</sup>. Radiation therapy is critical in cervical cancer treatment, and when combined with external beam radiation therapy, brachytherapy has been shown to improve local control and survival <sup>(4)</sup>. With the increased use of image-guided adaptive brachytherapy for cervical carcinoma, brachytherapy treatment planning has become increasingly personalized. This development has enabled interstitial applications to advance tumour target coverage while maintaining acceptable morbidity rates <sup>(5)</sup>. Image-guided brachytherapy describes how diagnostic

radiology is incorporated into the process of brachytherapy. Increased use of 3D treatment planning in the treatment of cervical cancer has improved oncological outcomes and reduced treatment-related toxicities <sup>(2)</sup>. The history of interstitial brachytherapy began in 1917 when Barringer inserted a radium needle into the prostate, guided via the rectum with a finger <sup>(6)</sup>. This can roughly be associated with 2D brachytherapy, in which 2D planar images are taken for treatment planning after the insertion of sources. For years, developments in technology in cervix carcinoma brachytherapy treatment were limited, and treatment was on 2D based imaging and conventional approaches were developed in the early twentieth-century by the brachytherapy fraternities. However, there is a major change in practice with the introduction of three-dimensional brachytherapy and image-guided brachytherapy <sup>(7)</sup>. The emerging technique has demonstrated a significant improvement in clinical results and dose volume parameters, owing largely to the high precision with dose delivery. <sup>(8)</sup>

## 1.2 *Problem statement*

At Komfo Anokye Teaching Hospital (KATH), two-dimensional Low dose rate brachytherapy is the approach used for cervix carcinoma boost treatments. For 2D brachytherapy, the treatment design is based on a small number of points determined from the patient's 2D planar images. Also there is a limitation in the imaging modality used in brachytherapy as it utilizes planar radiographs obtained from radiotherapy simulators. This is the main limitation of brachytherapy treatment planning at the hospital as there is an inadequate spatial information of the tumour and Organs at Risk (OAR) volumes and thus the inability to visualize the extent of the tumour and applicators in 3D, resulting in suboptimal planning of the application technique with inadequate dose coverage to large tumours. This brachytherapy technique has been executed conventionally

by the prescription of the radiation dose to a geometrical point A <sup>(9)</sup>. The size of the tumour is not taken into account, nor are the positions and shapes of the surrounding organs at risk with this type of treatment. As a result, some patients are likely to receive less optimal brachytherapy treatment than they would have received with personally tailored 3D brachytherapy.

### 1.3 *Relevance and justification*

The transition from conventional to MRI-guided adaptive brachytherapy, and from 2D brachytherapy is presumed to produce unique advantages. Improvement in local control was highly observed in patients with large tumours receiving significant tumour dose escalations of > 10 Gy, most notably through needle use, and who also had the major residual disease at the period of brachytherapy. (*Kari Tanderuo Ph.D. Et. 2004 Magnetic Resonance Imaging in Oncology*). Although 2D brachytherapy involves no image guidance, it has its own advantages. It enables precise localization and immobilization of the tumour, thereby avoiding the complications associated with set-up errors and the movement of organs associated with external beam radiotherapy <sup>(10)</sup>. On the other hand, because Image-guided brachytherapy utilizes CT or MR imaging instead of 2D orthogonal radiographs, dosage is prescribed to target volumes rather than points of reference, as is with 2D brachytherapy. 3D High Dose Rate brachytherapy (3D-HDR-BT) is an image-guided technique developed from 2D-HDR-BT. In comparison to 2D-HDR-BT, this image-guided 3D-HDR-BT can deliver a high conformal dosage and more precise distributions.

Recent research has demonstrated that 3D-HDR-BT is effective in patients with cervical cancer, prostate cancer, and breast cancer following external beam radiotherapy treatment. 3D

HDR brachytherapy describes the design and delivery of radiotherapy treatment plans based on at least one 3D image dataset. The delivery consists of an HDR radioactive source stopping for short times at various dwell positions in an automated manner to treat only the target tissue.

#### **1.4 Scope of the study**

Recently, treatment planning systems in 3D are becoming prevalent in the majority of radiotherapy facilities. This technology enables radiation to be shaped spatially to conform to the target volume and dose to normal tissues to be reduced. This particular approach allows for a reduction in the likelihood of the normal tissue toxicity while increasing the dose to the tumour, resulting in higher rates of local control. Regardless of the wide use of three-dimensional image-based dosimetry in brachytherapy in highly resourced radiotherapy centres around the world, it is now being considered for implementation at KATH.

#### **1.5 Objectives of Study**

Magnetic resonance imaging, computed tomography, and ultrasonography are the considered standard imaging modalities for cervical cancers. Their application in image-guided brachytherapy is still progressing. Trans-abdominal ultrasonography can be used to determine the thickness, size of the uterus as well as its shape and diameter. It can be utilized in the guidance of proper placement of applicators to avoid inadvertent perforation of the rectum during difficult intracavitary brachytherapy insertions. Additionally, it has been used to establish the relative positions of the bladder and rectum during gynecological applications in brachytherapy. The determination of dose to the rectum and bladder, cavities by ultrasound localization are more often greater than those calculated using conventionally defined dose specification points. There is also

the utilization of trans-abdominal intraoperative ultrasonography for guidance during interstitial implantation of gynecologic malignancies. It is especially useful for the guide of needles near the bladder and the determination of the depth of needle insertion. Trans-rectal ultrasound is frequently used in prostate brachytherapy to guide interstitial implantation of advanced gynecologic cancers and to avoid bladder and rectum perforation. Trans-rectal ultrasonography appears to be more effective at visualizing cervical tumours than trans-abdominal ultrasonography. Fluoroscopy facilitates parallel needle placement and assists in guiding the depth of needle penetration during interstitial implants because the needles are visible under fluoroscopy easily. It is also beneficial in ensuring proper placement of intracavitary implants, thereby avoiding the need for repositioning and repackaging ineffective applications. Dose calculations are also performed using fluoroscopy and orthogonal radiography.

In recent years, there is frequent utilization of magnetic resonance imaging (MRI) and computed tomography (CT) in three-dimensional breast tomography (BT) of cervical cancer. As radiation oncologists are rather conversant in the interpretation of CT-based treatment planning, there is the provision of valuable volumetric information such as the tandem position within the uterus, the thickness of the recto-vaginal septum, and the relationship between the bladder/recto-sigmoid and the applicator. More accurate delineation of organs at risk (OARs) is provided than in MRI and this enables optimized dose to OARs. In addition, parameters that have been used in the reporting system in the past (e.g. point A) are preserved. On the other hand, the difficulty to accurately identify the target volume with CT is observed in distinguishing between residual gross tumour volume (GTV) structures, the uterus, the cervix, and the vagina. Also, CT has a limited ability to define parametrial tumour infiltration. Computerized treatment planning software is available that use CT instead of radiography for the plan of brachytherapy insertions. These procedures localize

accurately intracavitary applicators and demonstrate their three-dimensional relationship anatomically to neighboring structures, hence, the acquisition of delivered dose to the tumour volume and adjacent organs. Normally, the scanning of patients involves the deposition of contrast material into the bladder and rectum or through a bladder catheter. The use of standard intracavitary irradiation applicators made of metal may cause streak artifacts on CT images, making it difficult to identify the tumour volumes, anterior rectal wall, and posterior bladder wall. With dilute contrast usage in the bladder and rectum, CT numbers are expanded, and with the selection of appropriate window settings, there is improved image quality and better visualization of organ boundaries. Numerous institutions have investigated the use of CT-compatible applicators to reduce the streaking artifact. However, due to their high cost and limited availability, these applicators have been used in only a few institutions. The thickness of the uterine wall and the nearness of the recto-sigmoid and bladder to the tandem can be determined by computed tomography. The technology has also been utilized to assess the inserted needle position in relation to the recto-sigmoid and bladder, as well as to guide interstitial implantation and define needle penetration depth. Although CT images have certain limitations, there is the difficulty in differentiating between the tumour and the surrounding structures when evaluating the tumour volume or determining where the cervix ends and the vagina commences. As a result, integrating information from MRI and clinical evaluation may enhance the contouring. When it comes to soft tissue visualization, magnetic resonance imaging outperforms CT. It allows for the differentiation of the tumour from the normal cervix and uterus, as well as the visualization of malignant intrusion into nearby tissues (parametria, vagina). The precise description of the tumour ensures appropriate tumour delineation, which guarantees that the target receives a suitable radiation dose, resulting in excellent control rates. In cervical brachytherapy, the Group European de Curiethérapie-European

Society for Therapeutic Radiology and Oncology (GEC-ESTRO) recommended that for target definition MRI would be more appropriate <sup>(11, 12, 13, 14)</sup>. In many ways, an MRI is considered superior to a CT scan. On the other hand, various survey findings revealed that MRI was increasingly scarce in many institutions. Furthermore, proper training and expertise are required for accurate contouring with MRI. Also, special MRI-compatible brachytherapy applicators are significantly more costly compared to applicators made of metal. None of the medical facilities in Ghana are known to have started the use of MRI to plan brachytherapy yet.



## **CHAPTER TWO**

### **2.0 LITERATURE REVIEW**

#### **2.1 *Clinical Outcomes from IGABT studies***

Several institutions have reported clinical outcomes for cervical cancer Image-guided brachytherapy. Vienna (156 patients) and Aarhus (140 patients) produced the largest accessible studies in 2014 with patients receiving GEC-ESTRO-recommended definitive 3D EBRT, MRI-guided brachytherapy, and concurrent chemotherapy in prospective clinical procedures <sup>(15)</sup>. In 3 years the actuarial local control rates in the Vienna and Aarhus series were 95 percent, 91 percent, and 100 percent for IB, 86 percent for IIIB, and 96 percent for IIB, respectively, based on stages in the Vienna series. Both Vienna and Aarhus demonstrated improved local control, resulting in a 30% (from 38% to 68%) and a 16% (from 63% to 79%) increase in overall survival in both series, respectively. In the two series, there was also evidence of considerable morbidity reduction when a comparison is done with historical controls <sup>(15)</sup>. Improved detection and treatment of positive lymph nodes, as well as the use of concurrent chemotherapy, are thought to have made significant contributions to improved survival even though given the extent of the improvement, the transition to MRI-guided adaptive brachytherapy is also thought to have contributed. Large tumours (stage IIIB, in particular through the use of needles in patients with significant residual disease at the time of brachytherapy, showed the most improvement in local control. In the use of MRI guidance, excellent results have been documented in vaginal cancer and recurring gynaecological cancer treated with interstitial brachytherapy <sup>(15)</sup>. Various mono-institutional publications, including the RetroEMBRACE research, have also shown that IGABT has beneficial results <sup>(16-24)</sup>. From International Federation of Gynecology and Obstetrics (FIGO), diseases of stage IB1 and IB2 had 3-year pelvic and local control rates of 98–100% and 96 percent,

respectively, with stage IIB diseases having 93–96% and 89–91 percent, respectively <sup>(16, 25)</sup>, whereas stage III/IVA diseases had more variable local and pelvic control rates ranging from 73–86 percent. When compared to historical cohorts, local and pelvic control improvements were related to an overall survival benefit of around 10% in the RetroEMBRACE study <sup>(25)</sup>; several mono-institutional reports also found a similar benefit. <sup>(16, 17, 21)</sup>. In RetroEMBRACE and EMBRACE I, major morbidity in all Grade 3 to Grade 5 (G3-5) was reduced to 3–6% per organ after IGABT <sup>(25-27)</sup>. In the prospective French STIC research, 3D brachytherapy was observed to have a 50 percent decrease in 3 and 4-grade morbidity when it was compared to 2D brachytherapy <sup>(22)</sup>, making it similar to mono-institutional cohorts <sup>(16, 17, 20, 21, 28)</sup>. While significant morbidity is minimal, patients and physicians report minor morbidity on a regular basis <sup>(25, 26, 29, 30)</sup>, which has an effect on the quality of life <sup>(31)</sup>.

## **2.2 Target volumes, Dose and OARs**

There was insufficient evidence when the EMBRACE I study began recommending to all centers certain specific dose constraints to follow for organs at risk (OARs) and targets. As a result, there was the allowance of a wide range of institutional practices in terms of dose set objectives, applicators, intracavitary/interstitial techniques, prescribed dose, dose rate, and fractionation. Even though uniform volume contouring <sup>(32, 13)</sup> and dose-volume reporting were obligatory according to the GEC-ESTRO recommendations, dose delivery was heterogeneous <sup>(33, 14)</sup>. The variations in inter-institution and inter-patient dose of the RetroEMBRACE and EMBRACE I research presented opportunities to investigate the impact of variation in dose levels and procedures. A lot of mono-institutional studies, including the STIC study, utilized the recommendations by GEC-ESTRO in terms of volume selection, contouring, and reporting, allowing for comparing between

studies and institutions. IGABT research from mono-and multi-centres has been through the development of a large amount of new information on dose and volume impact correlations for targets and Organs at Risks <sup>(34)</sup>. Verification was done by GEC-ESTRO to the response-adapted target volume concept by the study of local failure patterns in the EMBRACE I study, as it indicated that 98 percent of local failures occurred inside the CTVIR and CTVHR <sup>(35)</sup>. Data from the RetroEMBRACE showed a strong association between local control, dose, volume, and overall treatment time (OTT) to all target volumes including GTVres, CTVHR, and CTVIR <sup>(36)</sup>. A 7 week delivery of CTVHR dose of 85 Gy ( $\alpha/\beta = 10$ ), D<sub>90</sub> had an achievement of a 3-year local control rate of 94 percent in small targets (CTVHR 20–30 cm<sup>3</sup>), 93 percent in intermediate-sized targets (CTVHR 20–30 cm<sup>3</sup>), and > 86 percent in large targets (CTVHR up to 70 cm<sup>3</sup>) during brachytherapy. Equivalent degrees of local control for doses of 60 Gy and 95 Gy ( $\alpha/\beta = 10$ ; D<sub>98</sub>) are a necessity for CTVIR and GTVres, respectively. The generation of a CTVHR dose of 85 Gy ( $\alpha/\beta = 10$ ) is determined by the technique of brachytherapy using D<sub>90</sub>. This demonstration from RetroEMBRACE showed that there was a significant increase in local control with the use of intracavitary/interstitial (IC/IS) brachytherapy in large tumours without increasing morbidity <sup>(37)</sup>. In addition, the IGABT experience has offered risk factor analysis, including dose, as well as descriptive evaluations of morbidity temporal patterns. Vaginal morbidity, especially stenosis, is common <sup>(38)</sup> and is related to ICRU recto-vaginal point dose and external beam radiation (prescribed pelvic dose) <sup>(39)</sup>. These results raised doubts on the theory of the radio-resistance of the vagina, and indicate that dosimetric guidance based on evidence can be used to reduce vaginal dose and morbidity <sup>(40)</sup>. Furthermore, the contribution of the revised vaginal dose reporting recommendations on for the mid and low vaginal regions has resulted in enhanced vaginal tissue sparing from excessive irradiation. <sup>(41, 42)</sup>. It was also established in the rectal morbidity analysis

of the EMBRACE I study that rectal morbidity is not that common with IGABT in grade 4 and grade 3 <sup>(42)</sup>; which demonstrates dose effect relationships for rectal morbidity <sup>(29, 42-46)</sup> and limitation resulting in a reduction in the incidence of grade 2 (G2) or proctitis and more bleeding to 5.2 percent and 4.6 percent, respectively, with the limitation of the rectal  $D_{2cc}$  to 65 Gy  $D_{2cc}$  to  $\leq 75$  Gy to decrease the incidence of fistulae to  $\leq 2.7\%$  <sup>(42)</sup>. Intermediate dose to larger volumes of the rectum can predict rectal morbidity (e.g V55 Gy) <sup>(47)</sup>. Dose-and-effect relationships are demonstrated in mono-institutional analysis for the bladder <sup>(41-45)</sup> and preliminary outcomes from EMBRACE I suggest an advantage in the limitation to the bladder  $D_{2cc}$  to  $\leq 80$  Gy. The bowels and sigmoid  $D_{2cc}$  are more likely to be related to stenosis, strictures, and fistulae <sup>(26)</sup>. Lastly, acute and late intestinal morbidities were related to the total volume irradiated to 43 Gy during EBRT <sup>(48-50)</sup>.

### 2.3 *IMRT versus IGABT*

Even with the evidence in intensity-modulated radiotherapy (IMRT), of the risk reduction of acute <sup>(50, 51)</sup> and late <sup>(52, 53)</sup> morbidities <sup>(54)</sup>, several institutions continue to use 3D conformal radiotherapy (3D CRT) for cervix cancer treatment, despite the fact that IMRT and VMAT have been available for many years. IMRT has been shown to reduce urine morbidity and help reduce the risk of bowel morbidity. Additionally, image-guided radiotherapy (IGRT) and its provision of a tight margin for treatment has the potential to considerably reduce the overall volume treated with EBRT. Benefits of radiochemotherapy over radiotherapy has been extensively shown, with multiple studies and meta-analyses establishing the merits of event-free survival, overall survival, and pelvic control. <sup>(55-56)</sup>. During treatment, the number of cycles received for systemic control in high-risk patients

may be crucial, such as those with an advanced FIGO stage or positive nodes<sup>(57)</sup>; hence, administering 5–6 cycles of chemotherapy at the maximum dose may reduce the risk of a distant metastases. According to these findings, early analysis from EMBRACE found that node-positive and advanced-stage patients who had 4 chemotherapy cycles experienced more systemic relapses than those who had 5 cycles <sup>(58)</sup>. Overall, there was a low nodal failure rate in the EMBRACE I study of about 11%, with fewer failures in patients with the absence of pathologic nodes at diagnosis compared to node-positive individuals (7 percent and 16 percent, respectively) <sup>(59)</sup>. 81 percent of node-positive patients at the time of diagnosis had a restriction of pathologic nodes to the pelvis (parametrium, internal/external iliac, including the obturator region, and common iliac). Some regions like the cranial pelvic field boundary and the para-aortic regions reported nodal failures at a rate of 71 percent <sup>(59)</sup>, compared to 58 percent in the pelvis. According to a study by Beadle et al. <sup>(60)</sup>, numerous regional recurrences (42%) were identified marginal to the irradiated volumes, around the cranial edge of the elective pelvic fields in particular. The launcher of the EMBRACE II study was in response to the positive results produced by the EMBRACE study and research group in IGABT, with the use of evidence-acquired treatments derived from the first two EMBRACE trials. EMBRACE II trial had the objectives of prospectively confirming the findings of the RetroEMBRACE and EMBRACE I research, as well as establishing a standard for improved overall survival, nodal, and systemic control, based on: improved local disease control, decreased morbidity, and enhanced quality of life. In balancing manageable morbidity with the target of high local control, the dose-effect relationships presented previously justify the utilization of a regimen of specific dose prescription for the primary tumour targets and OARs. In EMBRACE facilities that primarily perform intracavitary brachytherapy, D<sub>90</sub> doses of less than 85 Gy was delivered to 50% of patients with CTVHR volumes greater than 30 cm<sup>3</sup>. Increased use of intracavitary or

interstitial brachytherapy, which contributes to the achievement of dose restrictions for both targets and organs at risk is a change in practice<sup>(40, 61-63)</sup>. Furthermore, a proportion of patients treated to high doses, mostly with smaller tumours during brachytherapy and moderate CTVHR (30cm<sup>3</sup>), had low local tumour control. As a consequence, there is the possibility of lowering the dose in these patients as well as the OAR dose. Considering the relationship between vaginal morbidity and the dose-effect, restricting brachytherapy dose to less than 65 Gy and the EBRT dose to 45 Gy for the ICRU recto-vaginal point expected to decrease G2 incidence or a vaginal stenosis increase from 21% to 14%.<sup>(38)</sup> A demonstration in a multi-centre on silicon studies observed that reducing source loading in the ovoids with an increase source loading in the tandem (and needles if used) is practicable without the compromise of dose to CTV<sub>HR</sub> and GTV<sub>res</sub><sup>(39)</sup>. For most clinical procedures, vaginal loading is relatively around 50% of normal standard loading patterns<sup>(39)</sup>. Vaginal loading could be reduced by 33%, resulting in a significant reduction in the ICRU recto-vaginal dosage<sup>(39)</sup>. Similarly, there are no significant variations amongst institutions in the definition of the EBRT lower field border<sup>(41)</sup>. With posterior-inferior border of the symphysis (PIBS)<sup>(40, 41)</sup> as a reference reduced the dosage from EBRT to the lower and mid vagina could be as a result of the increased knowledge of the lower EBRT target border through a well-defined target concept for EBRT and an exact vaginal dose reporting system relating to the lower EBRT target border.

#### 2.4 *Point A consideration*

There have been numerous systems developed to specify dose in cervical cancer treatment, but two are common, namely, the Manchester system and the ICRU system. As shown in Figure 2, doses to four points: A, B, bladder, and rectum is the distinguishing feature of the Manchester

system. OTT (Overall Treatment Time) is determined by the dose at point A, which is 2 cm lateral to the cervical canal and 2 cm superior to the cervical orifice. Point B is defined as 3 cm laterally from point A of the without displacement of the central canal. Point A moves with the canal, if the tandem moves it, but 5 cm from the midline is the fixed measurement of point B. The recommended ICRU system associates dose distribution with a target volume instead of a specific point. The utilization of point A as a reference for 2D LDR brachytherapy treatment is of low significance as ideal normal cervical and paracervical anatomy is not present in many clinical situations, either because of disease, obstetrical trauma, or old age. Considering studies on the compulsion of dose to point A, 76 percent still prescribe the dose to point A rather than to a 3D based volume, according to a US survey, and 52 percent use International Commission on Radiation Units and Measurement (ICRU) points instead of values from the dose-volume histogram when evaluating OARs, despite the fact that an increasing number of clinics perform CT prior to brachytherapy<sup>(64)</sup>. The goal of a stepwise approach based on a retrospective study of the use of standard library brachytherapy treatment plans based on the prescribed dose to point A towards the GYN GEC-ESTRO recommendations was an evaluation of the aspects of dosimetry when switching to individualized treatment plans from standard library ones based on images from the CT. According to the findings, the given treatment was mostly based on dose prescription to point A, with doses to OARs taken into account. After a more thorough examination of the theoretical possibilities of dose prescription to target volumes, it was implemented. ICRU Report 38 provided guidelines for recording and reporting dose points within adjacent normal tissues (bladder and rectum), and lymphatic system representative points were defined during the use of either low-dose-rate or high-dose-rate intracavitary therapy for the treatment of cervical cancer. This report provided a rational foundation for calculating,

recording, and reporting doses for the treatment of cervix cancer and other gynaecological malignancies. The use of Points A and B is discouraged by ICRU 38 because the exact meaning and definitions have not always been interpreted in the same way in different centers and even in the same center over time. These variations may result in significantly different values for the calculation of the dose rate to Point A<sup>(65)</sup>. As a result, if the prescribed dose to Point A is used to calculate the total time of application, different time values will be obtained depending on the method used to assign the prescription point. The primary goal of this report was to identify a volume encompassed by an absorbed dose level of 60 Gy as the appropriate reference dose level for low-dose-rate (LDR) treatments, which demanded the specification of the dimensions (width, height, and thickness) of the pear-shaped 60-Gy isodose reference volumes (Figure 1).

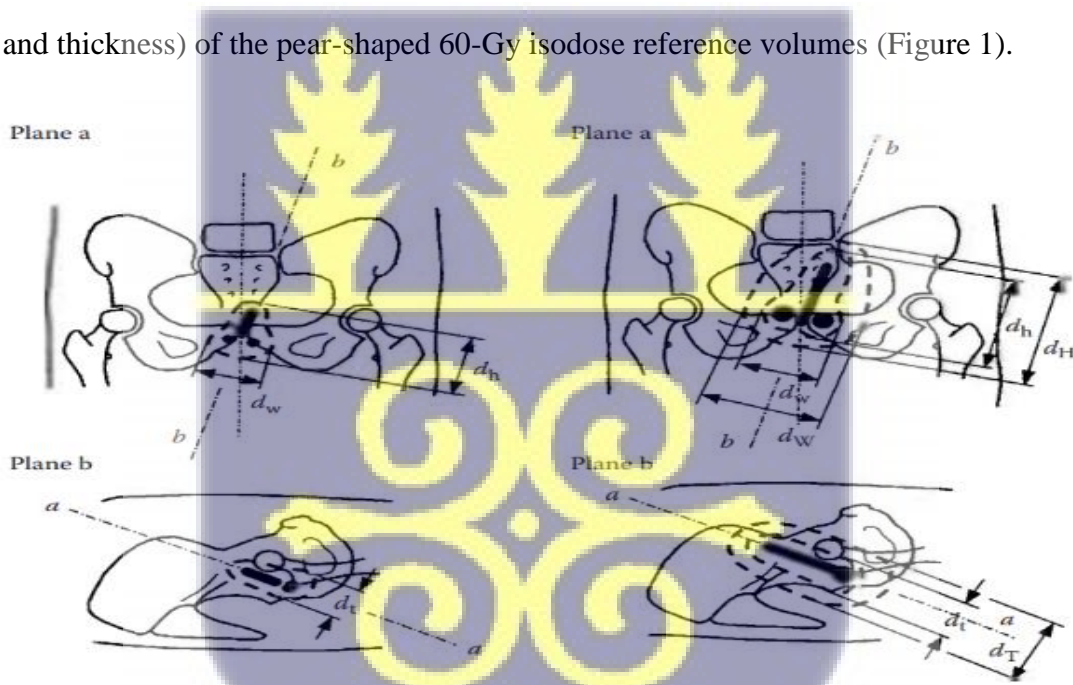
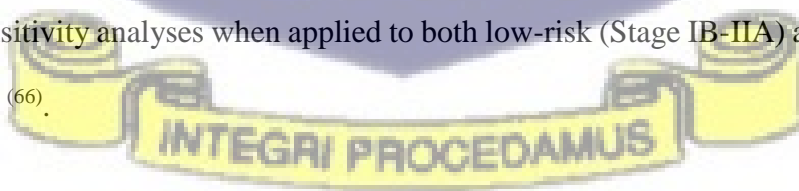


Figure 1. An implant patient's AP (planes a) and lateral (planes b) views are depicted in a schematic diagram of a 60-Gy dose. The width, length, and thickness of the 60-Gy dose isodose volumes are measured while accounting for external dose contribution.

## 2.5 2D LDR versus 3D HDR (cost)

The cost factor in our radiotherapy institutions is a required consideration during transitions to other treatment modalities, and there are quite a number of studies that direct the advantage to Image-guided brachytherapy practice as compared to 2D-LDR-BT which is now in use, especially at the KATH. From several studies, it has been shown that Image-guided brachytherapy is more cost-effective than 2D planning approaches for cervical cancer. A Markov model was used in a study by Kim et al to evaluate costs and results for a 5-fraction course of cervical brachytherapy utilizing 2D and IGBT procedures, with the cost of 5-fraction IGBT being \$21,374 (GHC 129,096.61) compared to 2D brachytherapy being \$17,931. (GHC 108,301.27). In the base case scenario, IGBT resulted in an increase of 0.16 QALYs (ICER = \$18,634/QALY). Using a \$50,000/QALY ICER threshold, the probabilistic sensitivity analysis preferred IGBT over 2D brachytherapy in 63 percent of model iterations. D'Souza et al. also conducted a cost-utility analysis for cervical cancer patients, comparing 2D brachytherapy to MRI-based brachytherapy, and discovered that MRI-based brachytherapy increased the anticipated QALYs by 0.35 and reduced lifetime treatment costs by \$1,892 when compared to 2D brachytherapy. Despite the fact that MRI-based brachytherapy is more expensive than 2D brachytherapy, lifetime costs were lower due to greater cancer control and decreased toxicity rates, lowering the predicted costs of recurring cancer and toxicity management. The aforesaid results were resilient on both probabilistic and deterministic sensitivity analyses when applied to both low-risk (Stage IB-IIA) and high-risk (IIB-IVA) subgroups. <sup>(66)</sup>



## 2.6 *Imaging modalities for IGABT*

Computed tomography was the initial imaging mode of choice for image-guided brachytherapy. The formation of streak artifacts was observed in the images as a result of the metallic applicators and tungsten shielding used in the ovoids. A CT-compatible LDR applicator was developed by Weeks and Montana at Duke and has become commercially available. A working group from Loyola University studied 19 women who had received implants. Initially, two-dimensional treatment planning was used, followed by a re-evaluation using CT-based three-dimensional dosage computation. When CT-defined cervix volumes are considered, there is a variation of 12 cm to 39 cm among women. More importantly, when the largest cervix cancer volumes were treated with the two-dimensional plan, the dose covering 90% of the cervix decreased to more than 40%. Similarly, Schroepel and colleagues from Michigan found a consistent underestimation of the dose to the cervix that was CT-visible by the dose to point A in all ten of their initial series cases. As a result, there is an improvement of dose to the cervix with the use of CT-compatible applicators and defined doses to organs at risk. Computed Tomography, however, may not be ideal for the determination of the extent of a disease, having 50 percent only to 65 percent accuracy in investigating the size and growth of cancer within the cervix, and also 75 percent to 80 percent precision in evaluating the parametrium in preoperative studies of early-stage patients<sup>(67)</sup>. The table below compares the advantages and disadvantages of the various imaging modalities used in brachytherapy planning of cervix carcinoma.

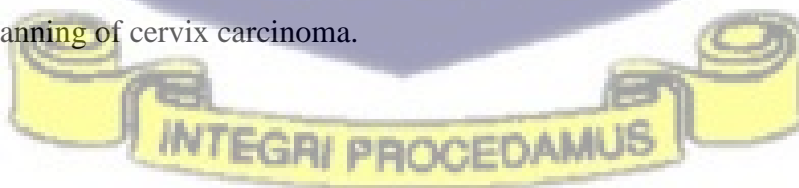


Table 1. Imaging modalities used for applicator and organ localization in cervix carcinoma and their effects on brachytherapy planning.

	STANDARD MODALITIES			FUNCTIONAL METABOLIC AND MODALITIES		
	PLAIN FILMS (2D)	COMPUTED TOMOGRAPHY (3D)	(T2) MRI 3D	FDG - PET	DCE - MRI	DW - MRI
Basis for target delineation	Landmarks based on applicator	3D X-ray attenuation	3D fluid density	Glucose metabolism	Tumour perfusion (low/heterogeneous = worse outcome)	Cellular density via diffusion restriction
Ability to delineate the primary	Poor	Moderate (overestimates)	Superior	Superior	Uncertain (may identify high risk volumes)	Uncertain (may identify high—risk volumes)
Ability to delineate normal tissue	Poor	Superior	Superior	Poor	Poor	Poor
Availability	All centres	Most centres	Few centres	Few centres	Few centres	Few centres

Clinical target volume (CTV) contouring is a weak point in the image-guided brachytherapy procedure chain. While both EBRT and BT have target contouring uncertainties, this limitation is much obvious in IGABT as a result of the sharp dose gradients observed in BT. Contouring is more reliant on the interpretation of "grey zones" at the moment. In terms of understanding the pattern of failure, the dose-volume-histogram (DVH) factors will be unreliable for treatment planning and later confounding if the target is not contoured to with the intent of reflecting the true localization of the macroscopic remains of the primary tumour during the period of brachytherapy. A reliable target definition is critical for the comparison of the parameters of DVH between departments and cooperating in trials from multi centers. The GEC-ESTRO Gynaecological Working Group defined some target definitions based on years of clinical experience interpreting tumour response during brachytherapy predominantly using MRI. In the area of tumour

contouring, MRI has clearly demonstrated dominance over CT. Although F18-fluorodeoxyglucose (18F-FDG) positron emission tomography-CT is being studied in this situation in other countries, the metabolic changes detected during EBRT may not be known to what degree of it being used for adaptive target definition (which may even disappear). There is a lack of data on the use of ultrasound, as well as a comprehensive target idea for ultrasound usage which is absent. The response of cervical tumours on MRI for use in the process of target contouring during EBRT when interpreted is not easy, even for other clinical personnel including, radiologists and radiotherapists. As a result, systematic interpretation and quantification of MRI findings are being developed in novel ways. When comparing experienced users, a high conformity index (0.7-0.8) has been recorded, whereas the conformity index for inexperienced observers has been shown to be much lower. 6 months and/or 30 patients of contouring experience is the least recommendation to centers planning to commence with the MRI-based approach. Certain experiences such as teaching courses, contouring workshops, and the dummy run, were recommended by the European Study on MRI-guided brachytherapy in advanced cervical cancer (EMBRACE) study. In order for such facilities to develop and retain the necessary contouring abilities, there should be a specific patient load at the facility <sup>(68)</sup>. Information on physiological organ movement and displacements of tissue caused by needle insertions should be provided. Intra-procedural imaging control and online dose planning are preferred although pre-procedural imaging-based targeting and dosimetry cannot achieve this goal. CT or ultrasound are mostly sufficient for guiding brachytherapy. IMRI-guided prostate brachytherapy is currently being tested for viability. Combining interactive computed imaging and IMRI allows for real-time tumour targeting, volumetric tumour treatment, and dosimetry. Similarly, there are advantages to using MRI for defining tumours surrounding structures, which results in better treatment of tumour and a decrease in complication rate. A

targeted drug delivery procedure is what is observed in Image-guided needle positioning within tumours. The injection of ethanol currently is commonly used for the ablation of tumour or vascular occlusion. Image guidance helps in two aspects of targeted drug delivery: positioning of the needle within the tumour target and secondly the monitoring of the injected material distribution within the tissue being treated. The activity of developing new methods of imaging that are precisely sensitive to bind them to detectable contrast agents. Some examples include ethanol's ability to directly detect if chemical utilization of MRI to selectively take images and identify the specific tumour antibodies using various isotope techniques. Despite the fact that there is potential in oncologic therapy to targeted drug delivery, the precise role of image-guidance beyond needle positioning is uncertain. <sup>(69)</sup> Some important aspects of brachytherapy must be considered for general image guidance especially in gynaecological BT, as well as additional attention required in future image-oriented research and development <sup>(70)</sup>. There is variation at both the institutional and personal levels due to the applicator placement near or into a tumour (Manchester, Paris, Stockholm, Fletcher, etc.), as well as differences in the intra-personal and inter-personal insertion of applicators. Since providing high quality images of all vital elements including applicators, potential source positions, Gross Tumour Volume (GTV), CTV, and adjacent organs at risk (OARs) is the inherent aim of BT imaging, BT images must be taken with the applicators in place. This complicated aim has significant implications to interactions between contouring of regions of interest, treatment planning (source position) and demand on images of applicators. Critical to use these imaging methods that, hence, have been integrated during the treatment planning process for specific organ sites (e.g., prostate, gynaecology, breast, for imaging GTV and OAR) and applicator type and mandated adapted solutions. To obtain suitable images, an effort in research and development is a requirement. The applicator has a significant impact on

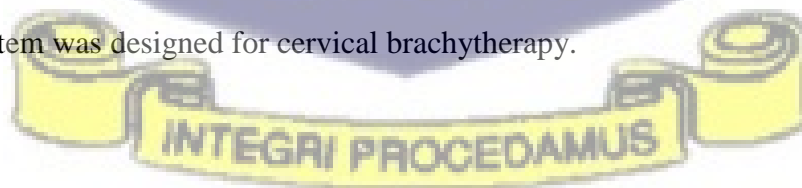
the adjacent topography in its relation to the Gross Tumour Volume, the tumour-bearing organ, and the adjacent OAR. It is associated with interstitial BT (oedema) and is the most noticeable in endoluminal intracavitary BT. Inter-application and inter-fraction uncertainty could be an implication, as impact varies by application and/or fraction during the same application. The identification of the source position(s) and applicators on the image in the individual patient (3D reconstruction) is the first step in BT treatment planning and it must be done precisely and precisely because the systematic error inherent in this procedure must be minimized in order to deliver high-quality BT.

Imaging in brachytherapy has a need for a systematic relationship between source and adjacent topography, implying a “Brachytherapy Eye View” (BEV) which is defined as a joint geometry system between the BT applicator and the image orientation of the patient, which is required for proper image guidance during applicator insertion, contouring of targets, reconstruction of applicators and treatment planning. If the specific characteristics of BT are considered, imaging plays an important role alongside clinical assessment at various stages in various ways within the treatment chain, such as image assistance in provisional treatment planning, image-guided application, image-assisted definitive treatment planning, and image-assisted quality control of dose delivery (imaging during/after brachytherapy). The importance of imaging and all related procedures cannot be overemphasized, as there is the requirement of great precision than orthodox EBRT as a result of very sharp dose fall-off in all directions, particularly in the adjacent region to the applicators used in brachytherapy. Target contouring has high effects on dose application as is seen to vary in millimetres. With the introduction of "In Room Imaging" for EBRT, consideration of a CT-scanner in the treatment room of necessary for brachytherapy, since imaging for the applicator in place can be done alongside GTV, CTV, and OAR. This implies

that "in-room imaging" is imaging with the applicator in place to some extent. However, the similarity to the situation during brachytherapy irradiation may be of significance to certain organs with significant motion relevant to brachytherapy, which appears to be minimal in certain situations for the stable relationship between the organs. Due to specific growth patterns and different configurations of treatment response, there may or may not be significant changes in tumour and EBRT will be fractionated along a fractionated course. Some significant changes occur in the pre-brachytherapy EBRT/chemotherapy case in cervix carcinoma, where the tumour may shrink with time. Hence, During the 40–50 Gy EBRT to the GTV in cervix cancer, its volume is reduced by 20–30% at the time of diagnosis. The situation at diagnosis, as well as the volume of tumour and configuration, are accounted for in IGABT as presented during the brachytherapy period with the applicators inserted into the tumour, based on images at diagnosis. Image-guided brachytherapy takes into account both spatial (3D) and time (4D) domains. Higher doses are obtained during BT using the response-adapted CTV than with EBRT currently <sup>(71)</sup>.

## 2.7 Dose specification

Until computer-based dosimetry systems became available, the Manchester system was one of the most commonly used brachytherapy systems (Figure 2). It was the first system to try to define dosimetry in terms of specific reference points. In terms of dose prescription to a point, known as Point A, this system was designed for cervical brachytherapy.



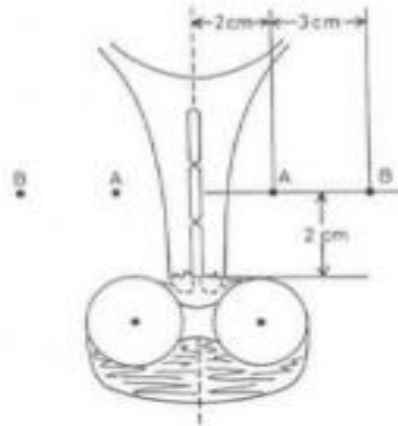


Figure 2. A diagram illustrating the geometric points A and B.

Selection of this point enabled the investigators to perform the following:

- Standardized the treatment of one patient with another.
- This point was located in a relatively low dose gradient area. Therefore, dose to this point was not oversensitive to minor changes in the position of the applicator.
- Relate the dosage to point A to the clinical outcomes. In order to achieve this goal, a set of applicators and loading schemes (i.e., the amount and distribution pattern of source in the applicator) were designed to create the same dose rate independent of the applicator arrangement. Point A has a relation to the paracervical triangle at the medial edge of the broad ligament where the crossing of the ureter and the uterine vessels are observed. It is worth noting that this is only a geometrical measurement representing the position of the pelvic sidewall nodes. The true position of these nodes varies among patients. The Manchester system developed rules for the activity, relationship, and positioning of the sources in the tandem and ovoids, resulting in the desired dose rate. Applicators in the

system were made up of a metallic tandem and two ovoids with diameters of 3 cm. Because there is no shielding in the ovoids, a generous anterior and posterior packing was required to reduce the dose to the bladder and rectum to acceptable levels. Standard insertion times were calculated for fixed applicator configurations and were not adjusted between patients unless the measured rectal dose was greater than the chosen tolerance value. The designated Manchester system plan for cervical cancer patients includes the following:

- Point A dose rate was similar for all allowed applicator loadings. This dose rate is for a perfect insertion and the severity of the disease frequently prevents the applicator from being perfectly inserted.

Manchester system plan for cervical cancer patients included the following:

- Point A dose rate was similar for all allowed applicator loadings. This dose rate is for an ideal insertion and the extent of the disease frequently prevents the applicator from being perfectly positioned. Regardless, even when the sources were moved, the dose rate at Point A for the "ideal" implantation determined the treatment time <sup>(72)</sup>.
- The vaginal contribution to Point A was restricted to 40% of the total dose.
- The rectal dose should be at least 80% of the Point A dose.

**NB.** The policy in the Manchester system was to measure the rectal dose with a probe. The tolerance dose to the rectum was taken to be 65% of the dose to Point A <sup>(73)</sup>.

In order to obtain homogenous dose distributions, sources with three different linear activities were utilized. The use of a specific pattern of radioactivity distribution was recommended depending on the shape (linear, planar, and volume implant) and size of the implant <sup>(73)</sup>. Paterson and Parker

devised a tabulation system for the required total source strength in milligram-hours (mg-h), as well as some recommendations for source distribution within each implant type, in order to achieve 1000 cGy (at the time with the unit "rad") at the prescription point. The Patterson– Parker dosimetry system was designed to plan and deliver a uniform dose (within 10% of the prescribed or stated dose) across the treatment area or volume.



## CHAPTER THREE

### 3.0 METHODOLOGY

Dosimetric analysis of image-guided brachytherapy, on which this thesis is primarily based, requires a phantom construction necessary for data collection and analysis. A water phantom was hence constructed to represent the pelvic region of a standard adult female for data collection.

### 3.1 *Materials*

The materials considered initially for the phantom construction included gelatin (for a ballistic gel phantom), candle wax, and beeswax. Gelatin was given initial consideration as it had enough merits, such as its similarity to soft tissue in the aspects of effective atomic number, electron density (0.95g) and mass density (1.3-1.4g), as well as low cost, ease of manufacture and accessibility. Many studies have been done using this particular phantom, especially with ultrasound studies. The phantom was left at room temperature for 9 hours after being constructed with gelatin, and it melted due to its sensitivity to temperature. It was also observed to be brittle and not as compact. The figures below show the constructed gelatin phantom and its melting stage.



Figure 1. Image of moulded gelatin



Figure 2. Image of gelatin 9 hours after moulding in room temperature.

Beeswax and candle wax are materials that have also been considered for phantom creation as seen in some studies as they also have some similarities to soft tissue. However, these materials were noted to be expensive, not readily accessible, as well as sensitive to temperature changes, which makes them another liability to the study, as the durability of the phantom is of the essence for a dosimetric study. Finally, the water phantom was considered for the construction of the phantom as it also has similar properties to soft tissue, is readily accessible, moderately expensive, and even though it requires some expertise to manufacture, it was readily available. Water is the reference medium for brachytherapy source dosimetry (Rivard et al. 2004) <sup>(74)</sup>. Pure, degassed water is defined in the TG-43U1 report (Rivard et al. 2004) <sup>(74)</sup> as composed of hydrogen and oxygen atoms having a mass density of  $0.998 \text{ gcm}^{-3}$  and a temperature of  $22^{\circ}\text{C}$  as the recommended water composition for reference dosimetry. A water phantom, on the other hand, has some limitations for radiation dosimetry experiments around the brachytherapy source. For example, the cost of detectors useful in the brachytherapy field, such as TLD or radiochromic films, and the fact that some detectors may not be water-proof detectors. Furthermore, because of the high dose gradients in their vicinity, accurate source-detector positioning is essential in the dosimetry of brachytherapy sources. Without the introduction of a solid medium, it is nearly impossible to suspend the source and detectors with the required accuracy in the water phantom. However, for this study, a waterproof ion chamber was used, which addresses the limitations mentioned above. A jig to hold the applicators and ion chamber for data collection was constructed, initially with wood as a prototype, as seen below in Figure. 3, and then with Perspex as seen in Figure. 5.

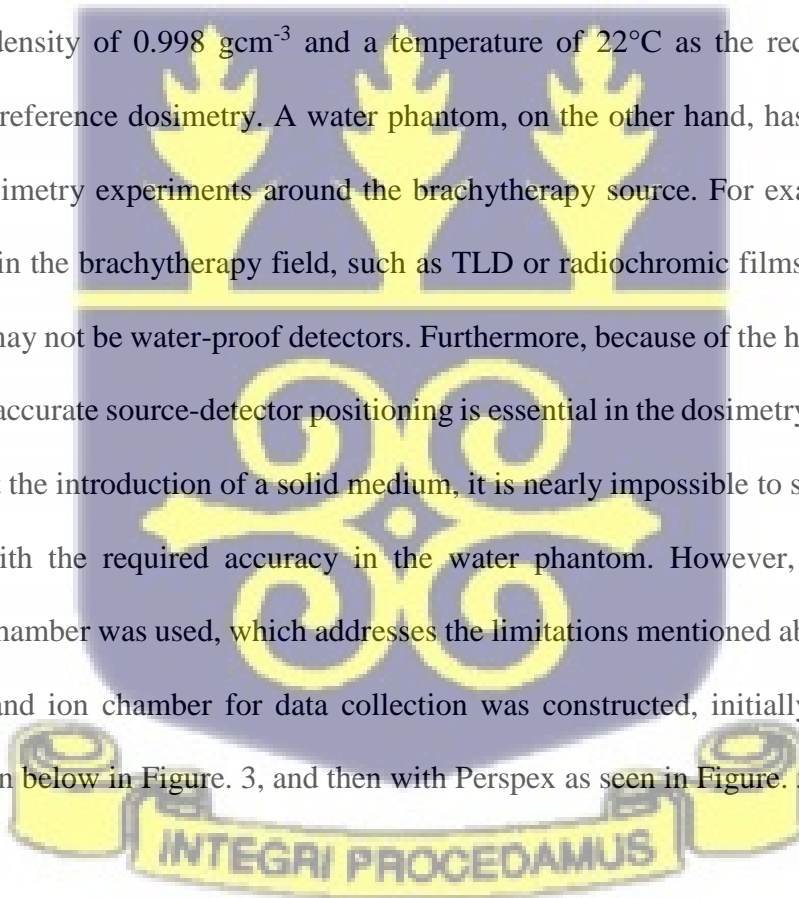




Figure 3. Image of the prototype of jig for water phantom made with wood.



Figure 4. Image of perspex of jig for water phantom used to hold applicators.

### 3.1.1 *Ionization chamber*

The ion chamber used for data collection in this study was a measuring assembly including an electrometer for the measurements of current or charge and a power supply for the ionization chamber's polarizing voltage, namely, the PTW 31010. This is a waterproof thimble ionization chamber utilized in high-energy photon and electron radiation measurement and is commonly used for the measurement of dose distribution in motorized water phantoms in therapy dosimetry. The PTW 31010 comes with an acrylic build-up cap for in-air measurements in a  $^{60}\text{Co}$  beam,

including a calibration certificate for absorbed dose in water or air kerma for  $^{60}\text{Co}$  beam energy. It has a vented sensitive volume of  $0.125\text{ cm}^3$  and is appropriate for water phantom data collection, with a flat energy response over a wide range of energies. The Model 31010,  $0.125\text{ cm}^3$  chamber has a given standard because of its measuring volume and spherical shape (IEC 2009). Typical distances of 2 cm, 5 cm, and 7 cm were used between the source and the ion chamber (five measurements were taken for each distance and results averaged). As a result of the PTW 31010 ion chamber being uncalibrated, a cross-calibration measurement was done with the A19 REF 92734 ionization chamber as its standard/ reference as it is the ion chamber in the department that had been calibrated.

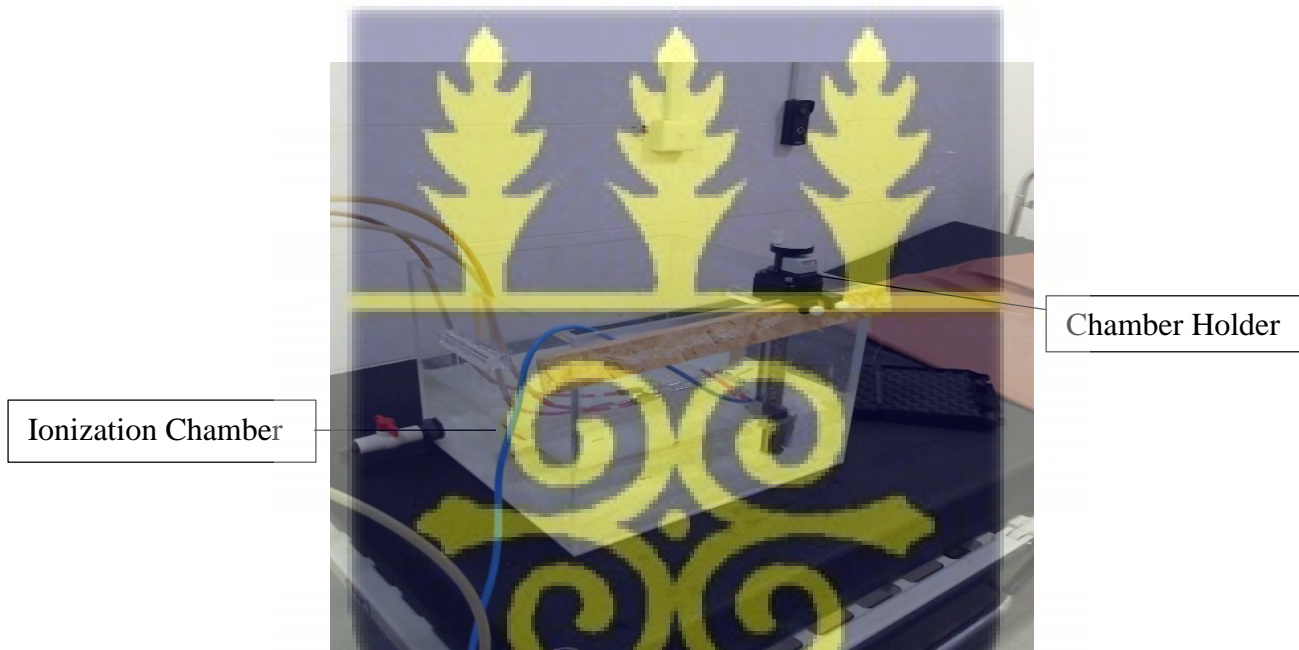


Figure 5. Image of calibrated ionization chamber in water phantom during taking data collection

### 3.1.2 Types of sources

$^{137}\text{Cs}$  is the most commonly used source for the treatment of gynaecological cancers. Most often, because it has different source strengths, which help to achieve the desired dose distribution.

However, a Cesium line source with a length of 17.2 mm is being used for cervical cancer patients with the 3D LDR treatment at KATH and hence for this study, due to its constant source energy and strength. The sources were three labelled U (source entering tandem into the uterus), V1 (source entering left ovoid in the cervix) and V5 (source entering right ovoids in the cervix) on the afterloader.

### 3.1.3 *Imaging*

Imaging is a vital aspect of this study. The imaging modalities considered for this study were ultrasound to guide the insertion of applicators and computed tomography for 3D treatment planning. As done before in the 2D brachytherapy procedure, a simulated image is acquired after the insertion of applicators for planning. Below is an image acquired at Komfo Anokye Teaching Hospital of a cervical cancer patient simulated after applicator insertion. The acquired image was used in the planning of the 2D LDR BT. However, for 3D-HDR-BT, CT images of the phantom (representing the pelvis of a cervical cancer patient) were taken and loaded onto the Eclipse treatment planning system where contouring was done on designated GTV, CTV, and PTV.

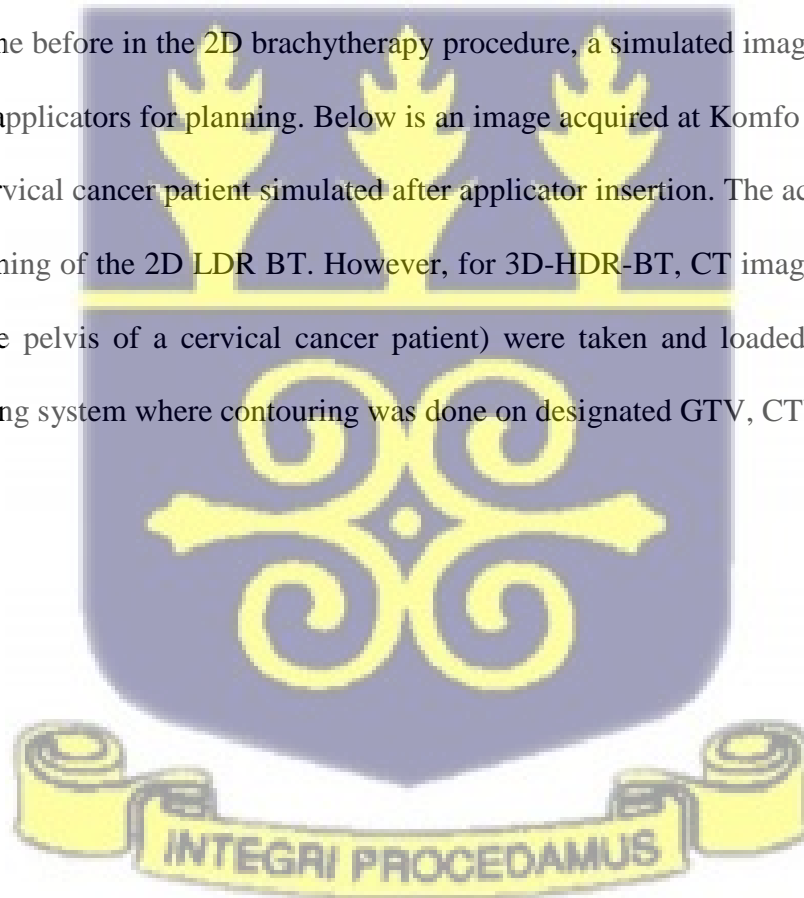




Figure 6. Scout CT image of the prototype water phantom showing jig with tandem and ovoids.

### 3.1.4 *Applicator system*

The Manchester system can be implemented in both 2D and 3D applicator insertions. Fletcher applicators with the after-loading property were used in the study with the source arrangement 1-3-5, which indicates the type, distance between sources, and positions of the sources in the applicators. Below is an image of the fletcher applicator.

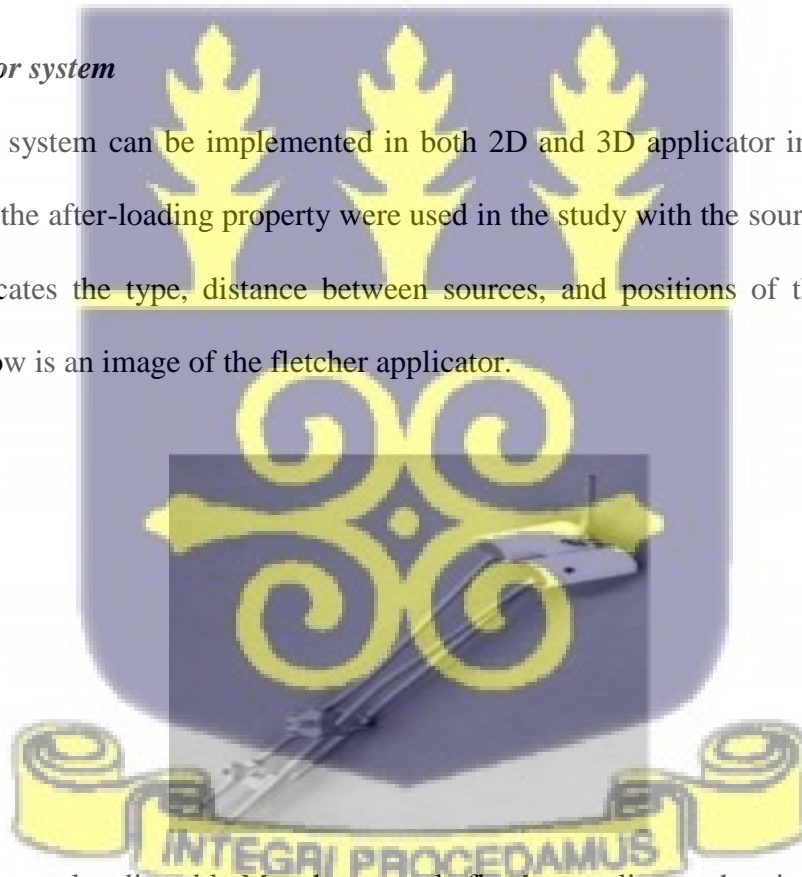


Figure 9. Modern style adjustable Manchester style fletcher applicator showing the tandem and ovoids.

### 3.2 Methods

#### 3.2.1 Phantom Design.

A water phantom with dimensions of 40 cm x 40 cm to represent the pelvic region of a standard adult female was considered for construction for data collection. Below are images of the design setup for the construction of the jig to hold the brachytherapy applicators and ion chamber during data collection as well as the water phantom.

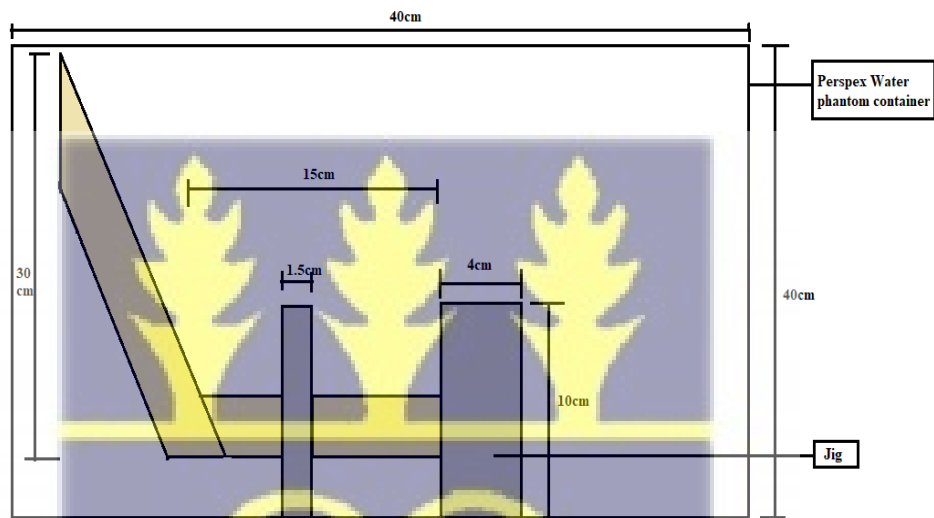


Figure 71. Side view of constructed the jig with dimensions in the Perspex water phantom container.

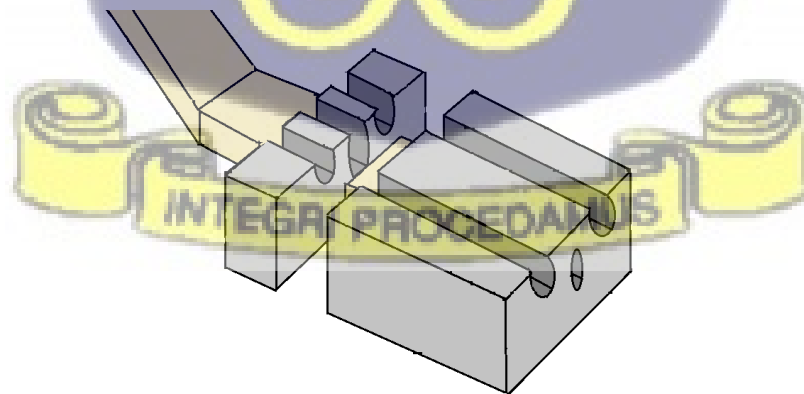


Figure 18. Block diagram of the jig used to hold the applicators in place in the water phantom.

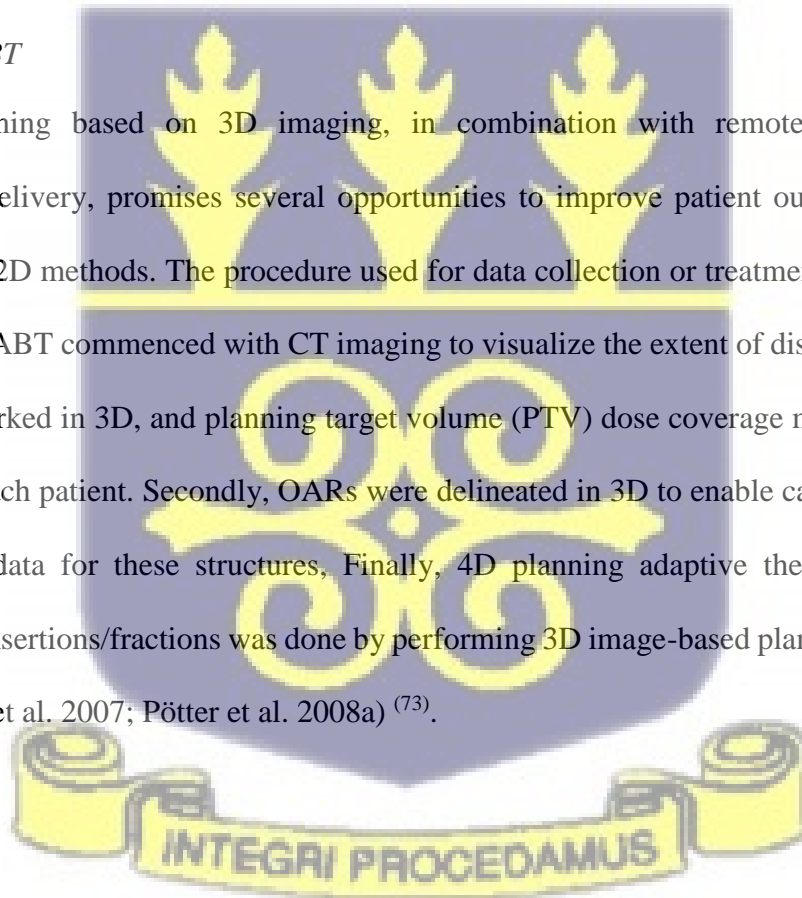
### **3.2.2 Treatment planning**

#### **3.2.2.1 2D LDR**

Treatment planning was done both in 2D LDR and 3D. After the insertion of applicators into the phantom, radiographs were employed to verify source placement and perform patient-specific dose calculations. After the source placements, manual calculations with the use of a calculator and a venier caliper. The parameters attained are imported into a software with the aid of a digitizer for further planning and verification of treatment time and dosage

#### **3.2.2.2 3D IGABT**

Treatment planning based on 3D imaging, in combination with remotely afterloading brachytherapy delivery, promises several opportunities to improve patient outcomes compared with traditional 2D methods. The procedure used for data collection or treatment planning in this study for 3D IGABT commenced with CT imaging to visualize the extent of disease and assumed CTV was be marked in 3D, and planning target volume (PTV) dose coverage marked to be more conformal for each patient. Secondly, OARs were delineated in 3D to enable calculation of dose-volume (D-V) data for these structures, Finally, 4D planning adaptive therapy for multiple brachytherapy insertions/fractions was done by performing 3D image-based planning prior to each irradiation (Lin et al. 2007; Pötter et al. 2008a) <sup>(73)</sup>.



### 3.2.3 Data Collection

#### 3.2.3.1 Dosimetry

Dose distribution across the water phantom was measured after the air kerma strengths of the sources were. Clinical dosimetry relies on a foundation of source calibration. The reference point for the source calibration is chosen to be at a distance of 1 cm from the source center ( $r_0 = 1$  cm, at  $\theta_0 = \pi/2$ ). Measurements to find the beam quality index ( $k_{Q,Q_0}$ ),  $M_{Q,Q_0}$  and CF (Correction factor) were conducted in order to convert the charge values recorded to dose (Gy). In calibrating for the beam quality, [ $k_{Q,Q_0} = k_{T,P} \times k_{POL} \times k_{SAT}$ ], temperature, pressure, polarity and ion saturation were corrected for. To find the correction factor of the ion chamber PTW 31010, CF ( $D_{A,Q}$ ) found to be proportional to  $\frac{M_S}{M_r} \times ND$ ; ( $D_{A,Q} = M_Q ND_{A,Q} k_{Q,Q_0}$ )<sup>(75)</sup>. With a half life of 30 years, the exposure rate of 137-Cs sources at 1m was calculated to be  $2.48 \times 10^{-09} \text{ Ckg}^{-1}\text{s}^{-1}\text{m}^{-2}$  and  $1.79 \times 10^{-09} \text{ Ckg}^{-1}\text{s}^{-1}\text{m}^{-2}$  for U and V sources, respectively. To determine the dose delivered by the sources, it was ideal to investigate the individual source strengths. Hence, the initial parameter considered for the dosimetric study was the air kerma strengths ( $S_K$ ) of the individual sources. The exact exposure rates at the various distances of 2 cm, 5 cm, and 7 cm from the sources were determined using  $X_I = 5.033 \times 10^{-08} \text{ Ckg}^{-1}\text{s}^{-1}\text{m}^{-2}$ ,  $1.504 \times 10^{-07} \text{ Ckg}^{-1}\text{s}^{-1}\text{m}^{-2}$ ,  $3.191 \times 10^{-07} \text{ Ckg}^{-1}\text{s}^{-1}\text{m}^{-2}$  respectively in order to calculate for the air kerma strengths ( $S_K$ ) which were then calculated using  $S_K = X_I \times l^2 \times (W/e)$ , where  $W/e$  is the energy expanded per unit charge released in air. The air kerma strength measurement was done using a three-point measurement system (considered 3 different distances) instead of a seven point measurement system (considers 7 different distances) as the values were observed to decreased sharply with increasing distance.

## **CHAPTER FOUR**

### **4.0 RESULTS AND DISCUSSION**

The radiation quantities measured were in terms of air kerma strength, ionization recombination and absorbed dose by using the radiation measuring instruments. The collected data are provided the appendix below.

#### **4.1 *Comparison of 2D&3D Imaging***

CT images give better information about soft tissue as compared to x-rays, which give better information about bony tissue or tissue with a high atomic number (z). Metallic applicators were used for the study, thus giving better images with x-ray (2D) while artifacts were observed with CT (3D), making planning difficult as the images were not clear enough. For CT/ MRI compatible applicators would be necessary to improve imaging for better planning. The images of both modalities are shown in Figure 14 below.



Figure 14. An axial CT image of the water phantom with metallic applicators showing the presence of artifacts.

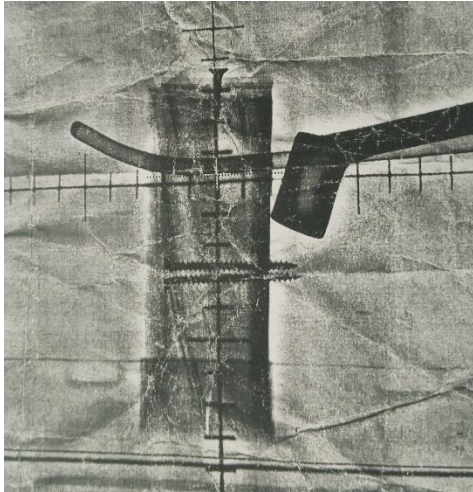


Figure 15A.

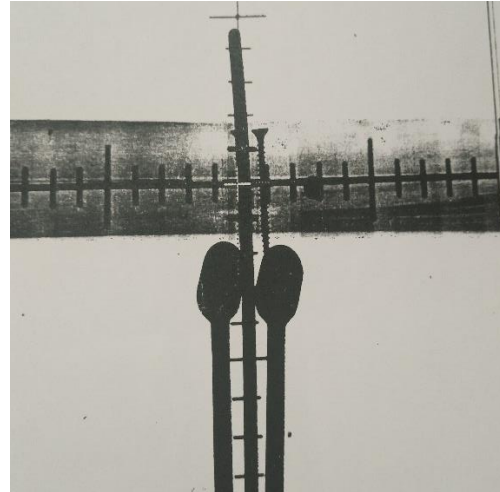


Figure 15B.

Figure 15. Planar X-ray radiographs of applicators within the water phantom: (A) lateral view and (B) anterior-posterior view (label the images (A) and (B)).

#### 4.2 Comparison of 2D&3D planning

Specific doses to the bladder and rectum were calculated. The doses to each organ were calculated for with optimized doses to the various organs using the same dose (44 Gy) prescribed to the CTV and PTV with contoured volumes of OARs in the 3D IGBT treatment planning. The DVH in the image below, *Figure 14*, gives information about the doses received by each organ volume after planning with doses delivered. Various organs are colour coded for easy identification, with the PTV, cervix and uterus being red, blue and yellow respectively, and the bladder and rectum being orange and pink, as seen in *Figure 16*.



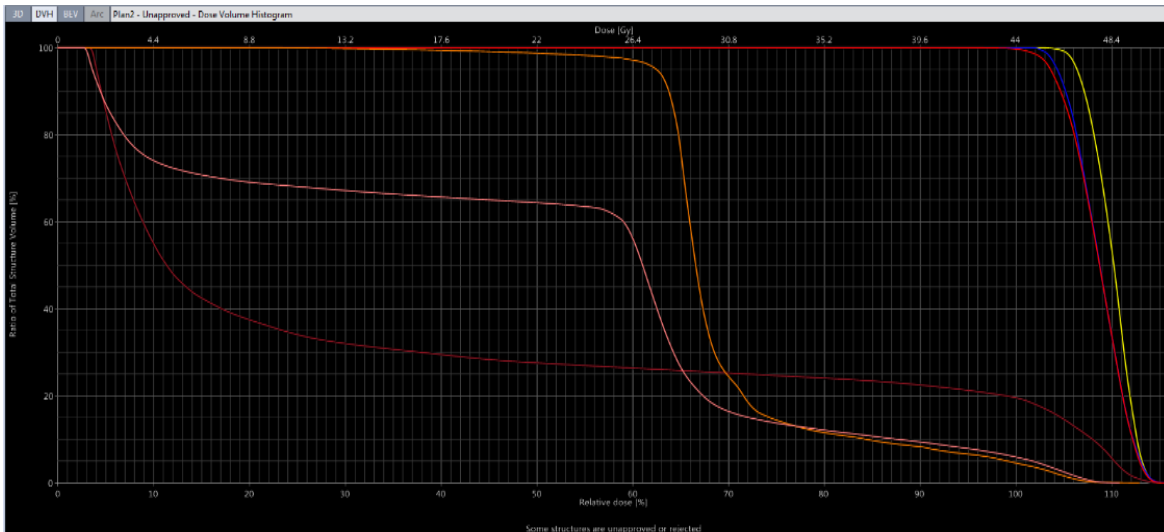


Figure 16. DVH showing doses received by various volumes of delineated organs.

With 3D IGBT treatment, planning made it easy to specify the dose for each volume with a tangible change in doses to go with the change in volumes. Listed in Table 2 are the prescribed doses to the various organs with their respective dose constraints and the differences between the dose delivered and the OAR constraints.

Table 2. Delivered doses and constraints during 3D treatment planning.

Organ Volume	Prescribed dose	Percentage delivered	Dose constraint of organ	% Gap from constraint
PTV	44 Gy	100%	No constraints	0%
Bladder	26.4 Gy	60%	80Gy	67%
Rectum	24.8 Gy	56.4%	75Gy	66.9%
Cervix	44 Gy	100%	No constraints (for cervix brachytherapy)	0%
Uterus	44 Gy	100%	No constraints (For cervix brachytherapy)	0%

### 4.3 Dosimetry

The air kerma strengths can be seen varying with distance in *Table 3* in Appendix 1 below.

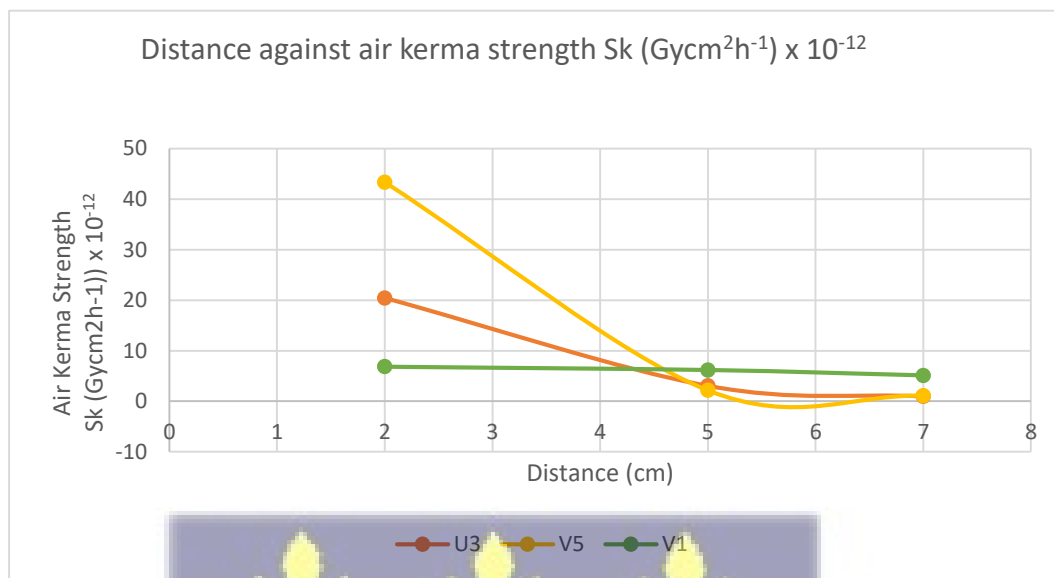


Figure 17. Graph of distance against air kerma strength  $S_k$  ( $\text{Gycm}^2\text{h}^{-1}$ )  $\times 10^{-12}$

$S_K$  (air kerma strength) for the three sources labelled V1, U3 and V5 at 2cm were  $6.839 \times 10^{-12}$   $\text{Gycm}^2\text{h}^{-1}$ ,  $2.043 \times 10^{-11}$   $\text{Gycm}^2\text{h}^{-1}$  and  $4.336 \times 10^{-11}$   $\text{Gycm}^2\text{h}^{-1}$  respectively. The second obtained parameter, dose distribution, was initially measured in ionized charges nC before being converted to dose. Nevertheless, the correction factor for PTW 31010 was not known, so the ion chamber was cross calibrated to the former type A19 ion chamber. The values attained for  $k_{Q_0}$ ,  $k_{T,P}$ ,  $k_{POL}$ ,  $k_{SAT}$  for cobalt were 8.892, 1.030, 0.975 and 8.854 respectively. The conversion factor ( $D_A, Q$ ) for PTW 31010 was determined to be  $3.240 \times 10^6 \text{ Gy/C} \pm 0.06$  and hence the doses at distances of 2 cm, 5 cm and 7 cm on the three different directions of exposure determined. The doses measured at 2 cm from the applicators' left, top, and right directions over a 300-second period were  $5.05181 \times 10^{-5}$  Gy,  $2.47082 \times 10^{-5}$  Gy, and  $6.13332 \times 10^{-5}$  Gy, respectively. First, the inverse square law ( $1/r^2$ ) is observed in the graph below, as there is a sharp dose fall as the distance from the source

increases. Secondly, a sharp dose fall out is observed after 2 cm from the source, which is identified as point A. The Manchester system's dose to point A is the system mostly used in 2D planning, which may not necessarily be of harm as a high percentage of the dose is observed to be deposited at 2 cm from the source. Nevertheless, at 5 cm from the source, doses are measured, implying exposure to OARs. Furthermore, the dose distribution in 2D is point-based and hence volumetric dose distribution is not considered as done in 3D, which implies that there may be doses beyond the 2 cm margin which are not accounted for during the planning, emphasizing the limitation of 2D treatment planning in brachytherapy.

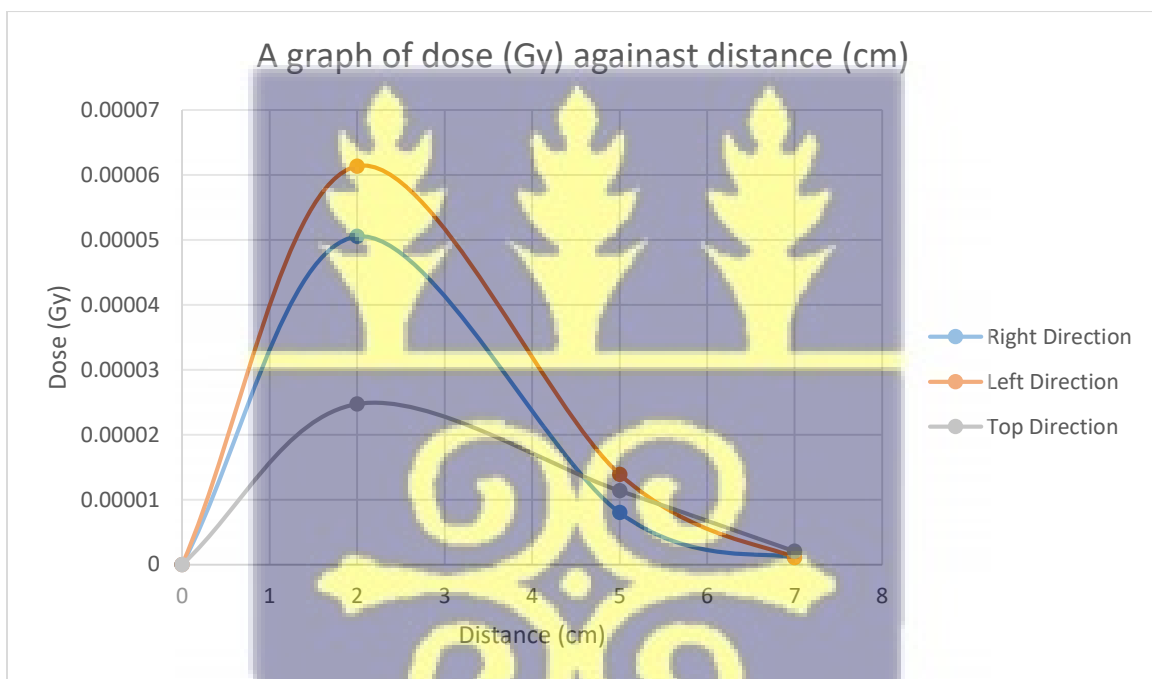
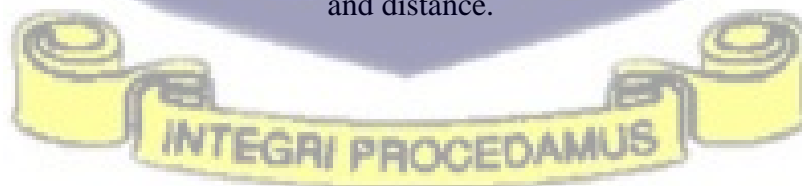


Figure 18. A graph of dose distribution in the water phantom showing the relation between dose and distance.



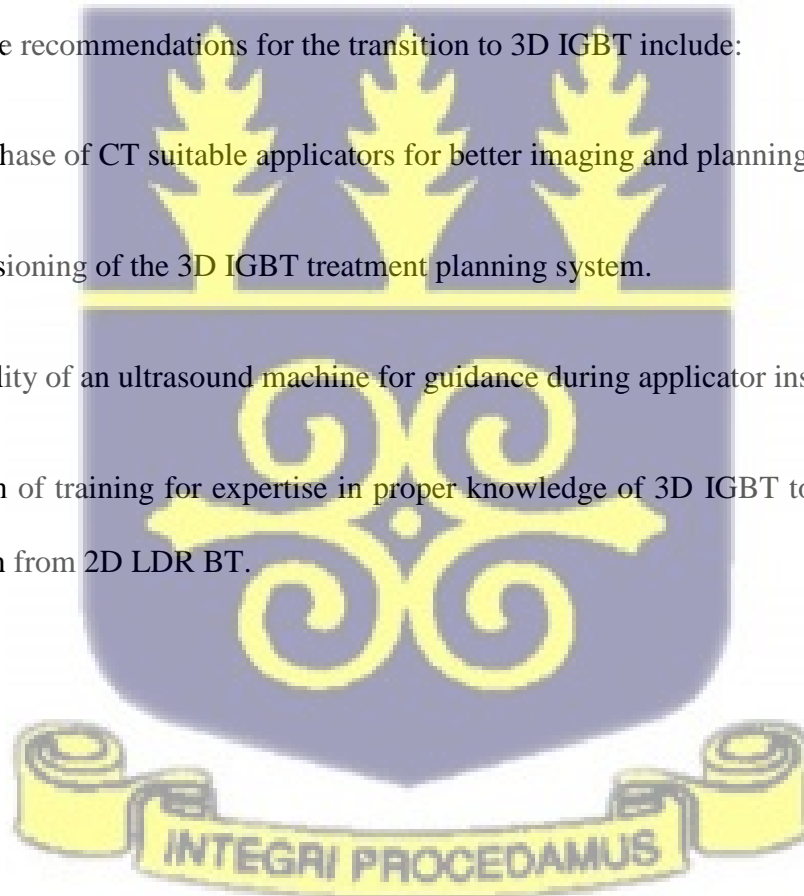
#### 4.4 Limitations

Due to the unavailability of the HDR source in the country during the period of the study, readings for 3D HDR were not measured. Hopefully, in the near future, this will be made available for further research. Also, the treatment planning system (TPS) for brachytherapy had not been commissioned yet, hence the EBRT TPS was rather used for the 3D planning for the brachytherapy water phantom.

#### 4.5 Recommendations

Regardless, some recommendations for the transition to 3D IGBT include:

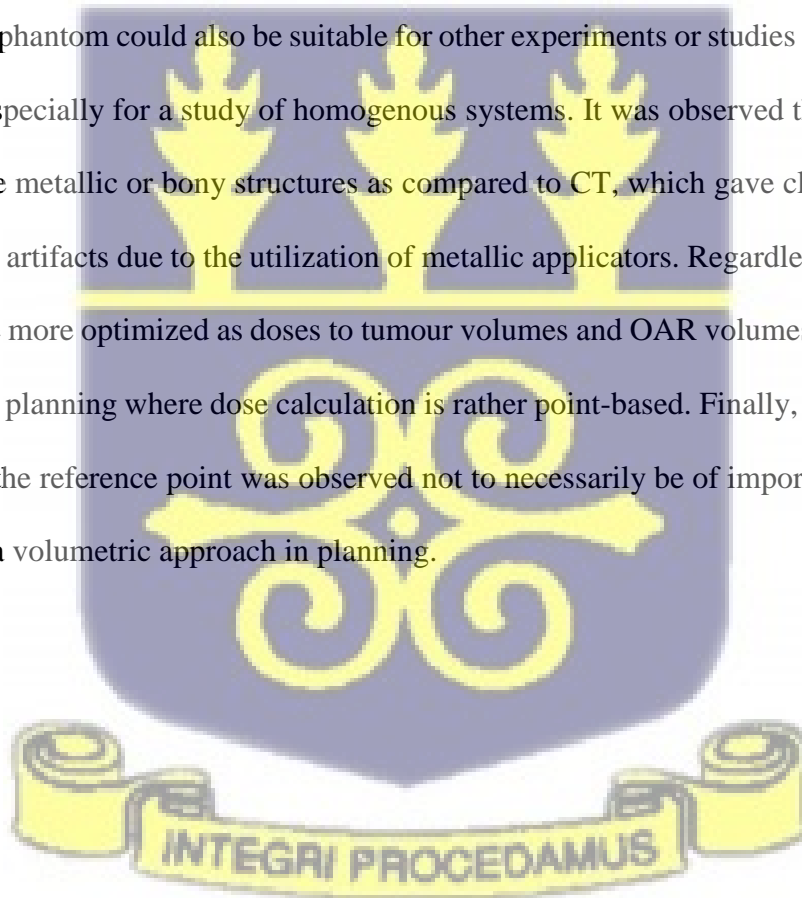
- The purchase of CT suitable applicators for better imaging and planning in 3D.
- Commissioning of the 3D IGBT treatment planning system.
- Availability of an ultrasound machine for guidance during applicator insertion
- Provision of training for expertise in proper knowledge of 3D IGBT to ensure a smooth transition from 2D LDR BT.



## CHAPTER FIVE

### 5.0 CONCLUSION

Over the years, certain developed countries have transitioned into this modality of treatment and have accumulated affirmative outcomes in the treatment of cervix carcinoma with brachytherapy. Even though 2D LDR may have come with some benefits, 3D Image-guided brachytherapy has been observed to be quite advantageous in imaging, planning, safety, and even cost. The successful construction of a water phantom was of importance in data collection and the comparison of data from both treatment modalities in brachytherapy made the variations between both modalities very clear. The water phantom could also be suitable for other experiments or studies involving external beam therapy, especially for a study of homogenous systems. It was observed that imaging in 2D highlighted more metallic or bony structures as compared to CT, which gave clearer images with tissues and more artifacts due to the utilization of metallic applicators. Regardless, planning in 3D is observed to be more optimized as doses to tumour volumes and OAR volumes are all accounted for, unlike in 2D planning where dose calculation is rather point-based. Finally, 2D LDR planning with point A as the reference point was observed not to necessarily be of importance in 3D IGBT since it follows a volumetric approach in planning.



6.0

**REFERENCES**

1. IAEA Human Health Reports *No.12*. (2015) The Transition from 2D brachytherapy to 3D High Dose Rate Brachytherapy. Pg 3.
2. Ann Barrett MD, Jane Dobbs MA, Stephen Morris MRCP, Tom Roques MRCP, Jonathan Harrowven Bsc., 2009. Practical Radiotherapy Planning, Vol. 4 Page 370.
3. CO/IARC Information Centre on HPV and Cancer, Ghana Human Papillomavirus and Related Cancers, Fact Sheet 2018. Pg 1.
4. Fang Wang, Senxiang Yan, et al. in Brachytherapy, 2017, Comparison of computed tomography and magnetic resonance imaging in cervical cancer brachytherapy: A systematic review. Pg 2.
5. Cervical Cancer. Antoine Schernberg MD, MSc, Cyrus Chargari MD, PhD et al, 2020 in Seminars in Radiation Oncology,. Pg 2.
6. H H Holm, Semin Surg Oncol. Nov – Dec, 1997. The history of interstitial brachytherapy of prostatic cancer. Pg 1.
7. The EMBRACE II study: The outcome and prospect of two decades of evolution within the GEC-ESTRO GYN working group and the EMBRACE studies. Clin Trans Radiat Oncol Vol 11(9) pg 48-60.
8. Pötter et al, 2021, in The Lancet Oncology, vol 22 Issue 4. Pg 538-547.
9. Gerbaulet A, Pötter R, Mazon JJ, Meertens H, Van Limbergen E. 2002. The GEC ESTRO Handbook of Brachytherapy. Brussels: European Society of Therapeutic Radiology and Oncology;
10. Ann Barrett MD, Jane Dobbs MA, Stephen Morris MRCP, Tom Roques MRCP, Jonathan Harrowven Bsc. 2009. Practical Radiotherapy Planning, Vol. 4. Page 54.
11. Hellebust TP, Kirisits C, Berger D, Pérez-Calatayud J, De Brabandere M, De Leeuw A, et al. 2010. Recommendations from Gynaecological (GYN) GEC-ESTRO Working Group: considerations and pitfalls in commissioning and applicator reconstruction in 3D image-based treatment planning of cervix cancer brachytherapy. Radiother Oncol; Vol 96. Pg 60-153
12. Dimopoulos JCA, Petrow P, Tanderup K, Petric P, Berger D, Kirisits C, et al. 2012. Recommendations from Gynaecological (GYN) GEC-ESTRO Working Group (IV): Basic

principles and parameters for MR imaging within the frame of image based adaptive cervix cancer brachytherapy. *Radiother Oncol*; Vol 103. Pg 22-113.

13. Hellebust TP, Tanderup K, Lervåg C, Fidarova E, Berger D, Malinen E, et al. 2013. Dosimetric impact of interobserver variability in MRI-based delineation for cervical cancer brachytherapy. *Radiother Oncol*; Vol 107. Pg 9-13.

14. Haie-Meder C, Pötter R, Van Limbergen E, Briot E, De Brabandere M, Dimopoulos J, et al. 2005. Recommendations from Gynaecological (GYN) GECESTRO Working Group (I): concepts and terms in 3D image based 3D treatment planning in cervix cancer brachytherapy with emphasis on MRI assessment of GTV and CTV. *Radiother Oncol*; Vol 74. Pg 45- 235.

15. Kari Tanderup PhD, Steven J. Frank MD et al, in *Seminars in Radiation Oncology*, 2014 C Magnetic Resonance Imaging in Radiation.

16. Lindegaard JC, Fokdal LU, Nielsen SK, Juul-Christensen J, Tanderup K. 2013. MRI guided adaptive radiotherapy in locally advanced cervical cancer from a Nordic perspective. *Acta Oncol*; Vol 52(15) Pg 9-10.

17. Ribeiro I, Janssen H, De Brabandere M, Nulens A, De Bal D, Vergote I, et al. 2016; Long term experience with 3D Image-guided brachytherapy and clinical outcome in cervical cancer patients. *Radiother Oncol*, Vol 120 Pg 54-447.

18. Nomden CN, de Leeuw AAC, Roesink JM, Tersteeg RJHA, Moerland MA, Witteveen PO, et al. 2013. Clinical outcome and dosimetric parameters of chemoradiation including MRI guided adaptive brachytherapy with tandem-ovoid applicators for cervical cancer patients: a single institution experience. *Radiother Oncol*; Vol 107. Pg 69–74.

19. Gill BS, Kim H, Houser CJ, Kelley JL, Sukumvanich P, Edwards RP, et al. 2015. MRI guided high-dose-rate intracavitary brachytherapy for treatment of cervical cancer: the University of Pittsburgh experience. *Int J Radiat Oncol Biol Phys*; Vol 91. Pg 7–540.

20. Rijkmans EC, Nout RA, Rutten IHM, Ketelaars M, Neelis KJ, Laman MS, et al. 2014. Improved survival of patients with cervical cancer treated with image-guided brachytherapy compared with conventional brachytherapy. *Gynecol Oncol*; Vol 135. Pg 8–231.

21. Charra-Brunaud C, Harter V, Delannes M, Haie-Meder C, Quetin P, Kerr C, et al. 2012. Impact of 3D image-based PDR brachytherapy on outcome of patients treated for cervix carcinoma in France: results of the French STIC prospective study. *Radiother Oncol*; Vol 103. Pg 13-305.
22. Tinkle CL, Weinberg V, Chen L-M, Littell R, Cunha JAM, Sethi RA, et al. 2015. Inverse Planned High-Dose-Rate Brachytherapy for Locoregionally Advanced Cervical Cancer: 4-Year Outcomes. *Int J Radiat Oncol Biol Phys*; Vol 92(10) Pg 93–100.
23. Castelnau-Marchand P, Chargari C, Maroun P, Dumas I, Del Campo ER, Cao K, et al. 2015. Clinical outcomes of definitive chemoradiation followed by intracavitary pulsed-dose rate image-guided adaptive brachytherapy in locally advanced cervical cancer. *Gynecol Oncol*; Vol 139. Pg 94–288.
24. Mahantshetty U, Krishnatry R, Hande V, Jamema S, Ghadi Y, Engineer R, et al. 2017. Magnetic resonance image guided adaptive brachytherapy in locally advanced cervical cancer: an experience from a tertiary cancer centre in a low-middle income country setting. *Int J Radiat Oncol*; Vol 99. Pg 17-608.
25. Sturdza A, Pötter R, Fokdal LU, Haie-Meder C, Tan LT, Mazon R, et al. 2016. Image-guided brachytherapy in locally advanced cervical cancer: improved pelvic control and survival in RetroEMBRACE, a multicenter cohort study. *Radiother Oncol*; Vol 120. Pg 33-428.
26. Jensen NBK, Kirchheiner K, Fokdal LU, Lindegaard JC, Kirisits C, Mazon R, et al. Bowel morbidity in cervix cancer after RCHT+IGABT; physician and patient reported outcome - EMBRACE. *Radiother Oncol* 2017; Vol 123. Pg 7-26.
27. Fokdal LU, Kirchheiner K, Kibsgaard Jensen N, Lindegaard JC, Kirisits K, Chagari C, et al. 2017. Physician assessed and patient reported bladder morbidity after RCHT and IGABT for cervical cancer. *Radiother Oncol*; Vol 123. Pg 4-23.
28. Sundset et al *Eur. J.* 2021. *Gynaecological Oncology*. Vol 42 (1). Pg 73-80.
29. Kang H-C, Shin KH, Park S-Y, Kim J-Y. 2010. 3D CT-based high-dose-rate brachytherapy for cervical cancer: clinical impact on late rectal bleeding and local control. *Radiother Oncol*; Vol 97. Pg 13-507.

30. Smet S, Najjari-Jamal D, Bk Jensen N, Fokdal L, Lindegaard JC, Kirisits C, et al. 2017. Fatigue, insomnia, hot flashes (CTCAE) after definitive RCHT+IGABT for cervical cancer (EMBRACE). *Radiother Oncol*; Vol 123 Pg 3-22.
31. Nesvacil N, Schmid MP, Pötter R, Kronreif G, Kirisits C. 2016. Combining transrectal ultrasound and CT for image-guided adaptive brachytherapy of cervical cancer: Proof of concept. *Brachytherapy*. Vol 15(6) Pg 44-839.
32. Petric P, Hudej R, Rogelj P, Blas M, Tanderup K, Fidarova E, et al. 2013. Uncertainties of target volume delineation in MRI guided adaptive brachytherapy of cervix cancer: a multi-institutional study. *Radiother Oncol*; Vol 107. Pg 6–12.
33. Pötter R, Georg P, Dimopoulos JCA, Grimm M, Berger D, Nesvacil N, et al. 2011. Clinical outcome of protocol based image (MRI) guided adaptive brachytherapy combined with 3D conformal radiotherapy with or without chemotherapy in patients with locally advanced cervical cancer. *Radiother Oncol*; Vol 100. Pg 23-116.
34. Tanderup K, Lindegaard JC, Kirisits C, Haie-Meder C, Kirchheiner K, de Leeuw A, et al. 2016. Image Guided Adaptive Brachytherapy in cervix cancer: a new paradigm changing clinical practice and outcome. *Radiother Oncol*; Vol 120. Pg 9-365.
35. Schmid M, Haie-Meder C, Mahanshetty U, Jürgenliemk-Schulz IM, Segedin B, Hoskin P, et al. 2017. Local failures after radiochemotherapy and MR-image-guided brachytherapy in cervical cancer patients. *Radiother Oncol*; Vol 123. Pg 26.
36. Tanderup K, Fokdal LU, Sturdza A, Haie-Meder C, Mazon R, van Limbergen E, et al. 2016. Effect of tumour dose, volume and overall treatment time on local control after radiochemotherapy including MRI guided brachytherapy of locally advanced cervical cancer. *Radiother Oncol*; Vol 120. Pg 6-441.
37. Fokdal L, Sturdza A, Mazon R, Haie-Meder C, Tan LT, Gillham C, et al. 2016. Image guided adaptive brachytherapy with combined intracavitary and interstitial technique improves the therapeutic ratio in locally advanced cervical cancer: analysis from the retroEMBRACE study. *Radiother Oncol*; Vol 120. Pg 40-434.
38. Kirchheiner K, Nout RA, Lindegaard JC, Haie-Meder C, Mahantshetty U, Segedin B, et al. 2016. Dose-effect relationship and risk factors for vaginal stenosis after definitive

radio(chemo)therapy with image-guided brachytherapy for locally advanced cervical cancer in the EMBRACE study. *Radiother Oncol*; Vol 118. Pg 6-160.

39. Mohamed S, Lindegaard JC, de Leeuw AAC, Jürgenliemk-Schulz I, Kirchheiner K, Kirisits C, et al. 2016. Vaginal dose de-escalation in image guided adaptive brachytherapy for locally advanced cervical cancer. *Radiother Oncol*; Vol 120. Pg 5-480.

40. Westerveld H, Pötter R, Berger D, Dankulchai P, Dörr W, Sora M-C, et al. 2013. Vaginal dose point reporting in cervical cancer patients treated with combined 2D/3D external beam radiotherapy and 2D/3D brachytherapy. *Radiother Oncol*; Vol 107. Pg 99–105.

41. Westerveld H, de Leeuw A, Kirchheiner K, Dankulchai P, Oosterveld B, Oinam A, et al. 2016. Multicentre evaluation of a novel vaginal dose reporting method in 153 cervical cancer patients. *Radiother Oncol*; Vol 120. Pg 7-420.

42. Mazon R, Fokdal LU, Kirchheiner K, Georg P, Jastaniyah N, Šegedin B, et al. 2016. Dose-volume effect relationships for late rectal morbidity in patients treated with chemoradiation and MRI-guided adaptive brachytherapy for locally advanced cervical cancer: results from the prospective multicenter EMBRACE study. *Radiother Oncol*; Vol 120. Pg 9-412.

43. Georg P, Pötter R, Georg D, Lang S, Dimopoulos JCA, Sturdza AE, et al. 2012. Dose Effect Relationship for Late Side Effects of the Rectum and Urinary Bladder in Magnetic Resonance Image-Guided Adaptive Cervix Cancer Brachytherapy. *Int J Radiat Oncol*; Vol 82. Pg 7-653.

44. Koom WS, Sohn DK, Kim J-Y, Kim JW, Shin KH, Yoon SM, et al. 2007. Computed tomography-based high-dose-rate intracavitary brachytherapy for uterine cancer: preliminary demonstration of correlation between dose-volume parameters and rectal mucosal changes observed by flexible sigmoidoscopy. *Int J Radiat Oncol*; Vol 68. Pg 54-1446.

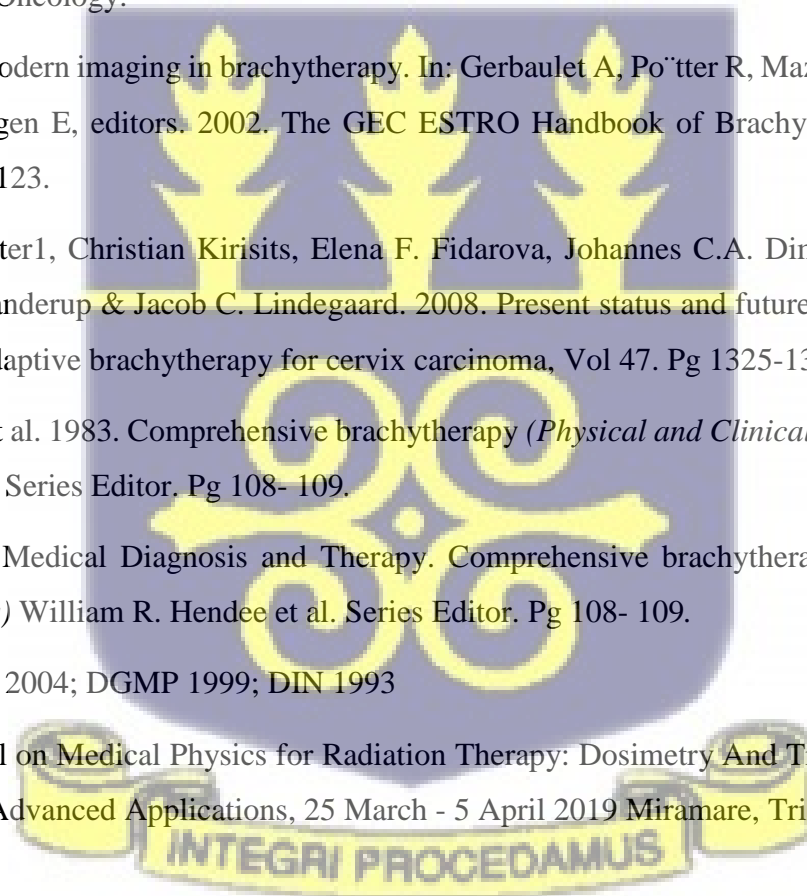
45. Mazon R, Maroun P, Castelnuovo-Marchand P, Dumas I, del Campo ER, Cao K, et al. 2015. Pulsed-dose rate image-guided adaptive brachytherapy in cervical cancer: dose-volume effect relationships for the rectum and bladder. *Radiother Oncol*; Vol 116. Pg 32-226.

46. Chopra S, Dora T, Engineer R, Mechanery S, Agarwal P, Kannan S, et al. 2015. Late rectal toxicity after image-based high-dose-rate interstitial brachytherapy for postoperative recurrent and/or residual cervical cancers: EQD2 predictors for Grade II toxicity. *Brachytherapy*; Vol 14. Pg 8-881.

47. Ujaimi R, Milosevic M, Fyles A, Beiki-Ardakani A, Carlone M, Jiang H, et al. 2017. Intermediate dose–volume parameters and the development of late rectal toxicity after MRI-guided brachytherapy for locally advanced cervix cancer. *Brachytherapy*; Vol 16. Pg 75-968.
48. Stanic S, Mayadev JS. 2013. Tolerance of the Small Bowel to Therapeutic Irradiation. *Int J Gynecol Cancer*; Vol 23. Pg 7-592.
49. Søndergaard J, Holmberg M, Jakobsen AR, Agerbæk M, Muren LP, Høyer M. 2014. A comparison of morbidity following conformal versus intensity-modulated radiotherapy for urinary bladder cancer. *Acta Oncol (Madr)*; Vol 53. Pg 8-1321.
50. Letschert JG, Lebesque JV, Aleman BM, Bosset JF, Horiot JC, Bartelink H, et al. 1994. The volume effect in radiation-related late small bowel complications: results of a clinical study of the EORTC Radiotherapy Cooperative Group in patients treated for rectal carcinoma. *Radiother Oncol*; Vol 32. Pg 23-116.
51. Naik A, Gurjar OP, Gupta KL, Singh K, Nag P, Bhandari V. 2016. Comparison of dosimetric parameters and acute toxicity of intensity-modulated and three dimensional radiotherapy in patients with cervix carcinoma: a randomized prospective study. *Cancer Radiothérapie J La Société Fr Radiothérapie Oncol*; Vol 20. Pg 6-370.
52. Mundt AJ, Mell LK, Roeske JC. 2003. Preliminary analysis of chronic gastrointestinal toxicity in gynecology patients treated with intensity-modulated whole pelvic radiation therapy. *Int J Radiat Oncol Biol Phys*; Vol 56. Pg 60-1354.
53. Chopra S, Engineer R, Mahantshetty UM, Dora T, Kannan S, Phurailatpam R, et al. 2015. Phase III RCT of Postoperative Adjuvant Conventional Radiation (3DCRT) Versus IGIMRT for Reducing Late Bowel Toxicity in Cervical Cancer (PARCER) (NCT01279135/ CTRI2012/120349): results of Interim Analyses. *Int J Radiat Oncol Biol Phys*; Vol 93. Pg 4.
54. Klopp AH, Yeung AR, Deshmukh S, Gil KM, Wenzel L, Westin SN, et al. 2016. A Phase III Randomized Trial Comparing Patient-Reported Toxicity and Quality of Life (QOL) During Pelvic Intensity Modulated Radiation Therapy as Compared to Conventional Radiation Therapy. *Int J Radiat Oncol*; Vol 96. Pg 3.
55. Reducing uncertainties about the effects of chemoradiotherapy for cervical cancer: individual patient data meta-analysis. *Cochrane Database Syst Rev* 2010:CD008285.

56. Green JA, Kirwan JJ, Tierney J, Vale CL, Symonds PR, Fresco LL, et al. 2005. Concomitant chemotherapy and radiation therapy for cancer of the uterine cervix. In: Green JA, editor. Cochrane Database Syst. Rev., Chichester, UK: John Wiley & Sons, Ltd; p. CD002225.
57. Schmid MP, Franckena M, Kirchheiner K, Sturdza A, Georg P, Dörr W, et al. 2014. Distant metastasis in patients with cervical cancer after primary radiotherapy with or without chemotherapy and image guided adaptive brachytherapy. *Gynecol Oncol*; Vol 133. Pg 62-256.
58. Fortin I, Jürgenliemk-Schulz I, Mahantshetty UM, Haie-Meder C, Hoskin P, Segedin B, et al. 2015. Distant metastases in locally advanced cervical cancer pattern of relapse and prognostic factors: early results from the EMBRACE study. *Int J Radiat Oncol*; Vol 93. Pg 8–9.
59. Nomden C, de Leeuw AAC, Tanderup K, Lindegaard JC, Kirisits C, Haie-Meder C, et al. 2016. Nodal failure after chemoradiation and magnetic resonance imaging guided adaptive BT in cervical cancer: a sub-analysis within embrace. *Int J Radiat Oncol Biol Phys*; Vol 96. Pg 12.
60. Beadle BM, Jhingran A, Yom SS, Ramirez PT, Eifel PJ. 2010. Patterns of regional recurrence after definitive radiotherapy for cervical cancer. *Int J Radiat Oncol Biol Phys*; Vol 76. Pg 403-1396.
61. Dimopoulos JCA, Kirisits C, Petric P, Georg P, Lang S, Berger D, et al. 2006. The Vienna applicator for combined intracavitary and interstitial brachytherapy of cervical cancer: clinical feasibility and preliminary results. *Int J Radiat Oncol*; Vol 66. Pg 83–90.
62. Kirisits C, Lang S, Dimopoulos J, Berger D, Georg D, Pötter R. 2006. The Vienna applicator for combined intracavitary and interstitial brachytherapy of cervical cancer: design, application, treatment planning, and dosimetric results. *Int J Radiat Oncol Biol Phys*; Vol 65. Pg 30-624.
63. Fokdal L, Tanderup K, Hokland SB, Røhl L, Pedersen EM, Nielsen SK, et al. 2013. Clinical feasibility of combined intracavitary/interstitial brachytherapy in locally advanced cervical cancer employing MRI with a tandem/ring applicator in situ and virtual preplanning of the interstitial component. *Radiotherapy Oncology*; Vol 107. Pg 8-63.
64. Viswanathan AN, Erickson BA. 2010. Three-dimensional imaging in gynecologic brachytherapy: A survey of the American Brachytherapy Society. *Int J Radiat Oncol Biol Phys*; Vol 76. Pg 9-104.

65. International Commission on Radiation Units and Measurements (ICRU). 1985. Dose and volume specification for reporting and recording intracavitary therapy in gynecology. Report 38 of ICRU, ICRU Publications, Bethesda, MD.
66. Charles C. Vu MD, Daniel J. Krauss MD, 2020. in Seminars in Radiation Oncology, Advances in Brachytherapy.
67. Junzo Chino MD, Angeles Alvarez Secord MD, 2013. in Surgical Oncology Clinics of North America, Practical Radiation Oncology for Surgeons.
68. Kari Tanderup PhD, Jacob C. Lindegaard DMSc, MD, 2010. in Seminars in Radiation Oncology, Adaptive Radiotherapy, Contouring Uncertainties.
69. Ferenc A. Jolesz, 2002. in Oncologic Imaging, Image-Guided Tumour Targeting for Diagnosis and Therapy in Oncology.
70. Po'tter R. Modern imaging in brachytherapy. In: Gerbaulet A, Po'tter R, Mazeron JJ, Meertens H, Van Limbergen E, editors. 2002. The GEC ESTRO Handbook of Brachytherapy. Brussels: ESTRO; Pg 51-123.
71. Richard Potter<sup>1</sup>, Christian Kirisits, Elena F. Fidarova, Johannes C.A. Dimopoulos , Daniel Berger , Kari Tanderup & Jacob C. Lindegaard. 2008. Present status and future of high-precision image guided adaptive brachytherapy for cervix carcinoma, Vol 47. Pg 1325-1336.
72. Wilkinson et al. 1983. Comprehensive brachytherapy (*Physical and Clinical Aspects*) William R. Hendee et al. Series Editor. Pg 108- 109.
73. Imaging in Medical Diagnosis and Therapy. Comprehensive brachytherapy (*Physical and Clinical Aspects*) William R. Hendee et al. Series Editor. Pg 108- 109.
74. Rivard et al. 2004; DGMP 1999; DIN 1993
75. ICTP School on Medical Physics for Radiation Therapy: Dosimetry And Treatment Planning For Basic And Advanced Applications, 25 March - 5 April 2019 Miramare, Trieste, Italy, Pg 35.



**APPENDICES**

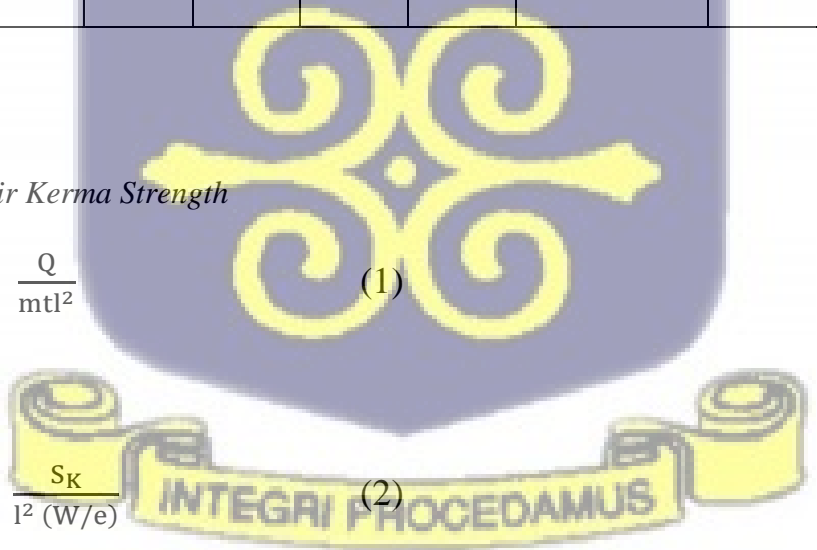
**7.0 Appendix 1: Air Kerma Strength**

Table 3. Charge, exposure rates and air kerma strength values of air kerma strength of sources V1, U3 and V5.

Source	Dist- ance (cm)	Charge (pc)					Average (pc)	Exposure rate $X_l(\mu\text{Ckg}^{-1}\text{s}^{-1}\text{m}^2)$	Air kerma strength $S_k(\text{Gycm}^2\text{h}^{-1})$
V1	2	6.030	6.010	6.040	6.060	6.060	$6.040 \pm 0.021$	$5.033 \times 10^{-08}$	$6.839 \times 10^{-12}$
	5	5.410	5.660	5.410	5.400	5.400	$5.456 \pm 0.114$	$7.275 \times 10^{-09}$	$6.178 \times 10^{-12}$
	7	4.900	4.500	4.500	4.120	4.500	$4.504 \pm 0.276$	$3.064 \times 10^{-09}$	$5.100 \times 10^{-12}$
U3	2	17.900	18.040	18.100	18.100	18.090	$18.046 \pm 0.090$	$1.504 \times 10^{-07}$	$2.043 \times 10^{-11}$
	5	2.730	2.700	2.680	2.690	2.700	$2.700 \pm 0.019$	$3.600 \times 10^{-09}$	$3.057 \times 10^{-12}$
	7	0.820	0.850	0.860	0.870	0.850	$0.850 \pm 0.019$	$5.782 \times 10^{-10}$	$9.625 \times 10^{-13}$
V5	2	38.540	38.140	38.140	38.140	38.500	$38.292 \pm 0.209$	$3.191 \times 10^{-07}$	$4.336 \times 10^{-11}$
	5	1.980	1.970	1.970	1.780	1.970	$1.934 \pm 0.086$	$2.579 \times 10^{-09}$	$2.190 \times 10^{-12}$
	7	0.980	1.090	0.980	0.980	0.980	$1.002 \pm 0.049$	$6.816 \times 10^{-10}$	$1.135 \times 10^{-12}$

*Calculation of Air Kerma Strength*

$$X_l = \frac{Q}{mtl^2} \quad (1)$$

$$X_l = \frac{S_k}{l^2 (W/e)} \quad (2)$$


$$S_k = X_l \times l^2 \times (W/e) \quad (3)$$

Where  $S_k$ ,  $X_l$ ,  $l^2$  and  $W/e$  represent air kerma strength, calibrated exposure rate of source, distance and energy expanded per unit charge released in air respectively.

Calculating for exposure rates of sources V1, V5 and U3 at 2cm.

$$X_l (V1) = \frac{6.040 \text{ pC}}{0.001\text{kg} \times 300\text{s} \times (2 \times 10^{-2})^2 \text{m}^{-2}}$$

$$= 5.033 \times 10^{-08} \text{ Ckg}^{-1}\text{s}^{-1}\text{m}^{-2}$$

$$X_l (V5) = \frac{38.292 \text{ pC}}{0.001\text{kg} \times 300\text{s} \times (2 \times 10^{-2})^2 \text{m}^{-2}}$$

$$= 1.504 \times 10^{-07} \text{ Ckg}^{-1}\text{s}^{-1}\text{m}^{-2}$$

$$X_l (U3) = \frac{18.046 \text{ pC}}{0.001\text{kg} \times 300\text{s} \times (2 \times 10^{-2})^2 \text{m}^{-2}}$$

$$= 3.191 \times 10^{-07} \text{ Ckg}^{-1}\text{s}^{-1}\text{m}^{-2}$$

$$S_k (V1) = X_l \times l^2 \times (W/e)$$

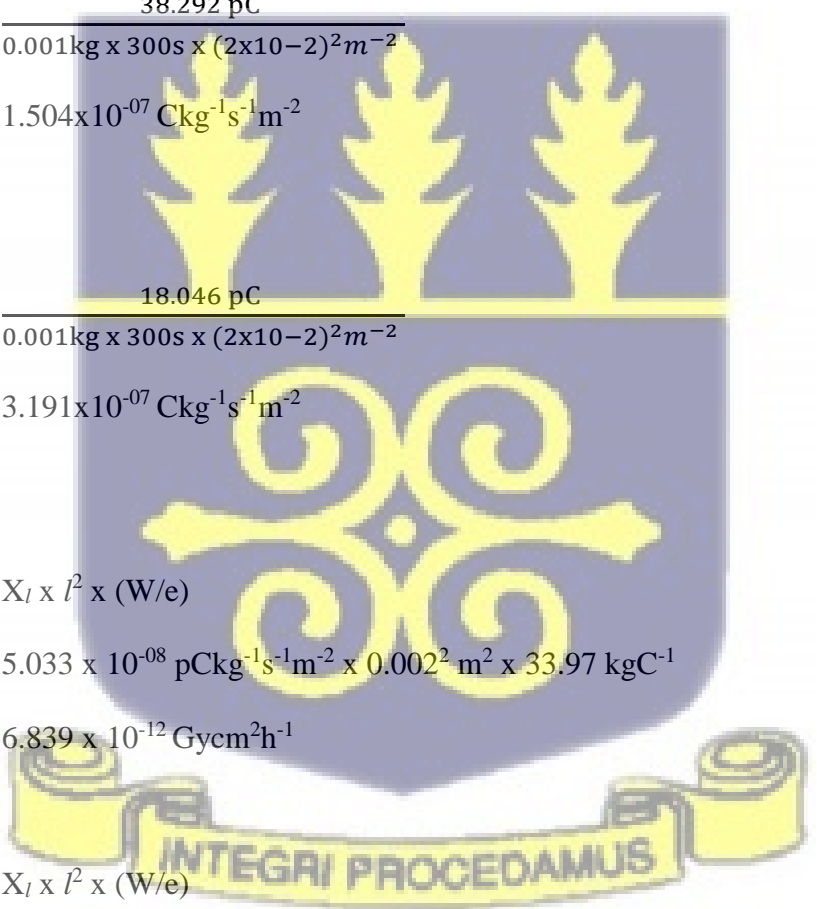
$$= 5.033 \times 10^{-08} \text{ pCkg}^{-1}\text{s}^{-1}\text{m}^{-2} \times 0.002^2 \text{ m}^2 \times 33.97 \text{ kgC}^{-1}$$

$$= 6.839 \times 10^{-12} \text{ Gy}\text{cm}^2\text{h}^{-1}$$

$$S_k (\text{Gy}\text{cm}^2\text{h}^{-1}) = X_l \times l^2 \times (W/e)$$

$$= 1.504 \times 10^{-07} \text{ pCkg}^{-1}\text{s}^{-1}\text{m}^{-2} \times 0.002^2 \text{ m}^2 \times 33.97 \text{ kgC}^{-1}$$

$$= 2.043 \times 10^{-11} \text{ Gy}\text{cm}^2\text{h}^{-1}$$



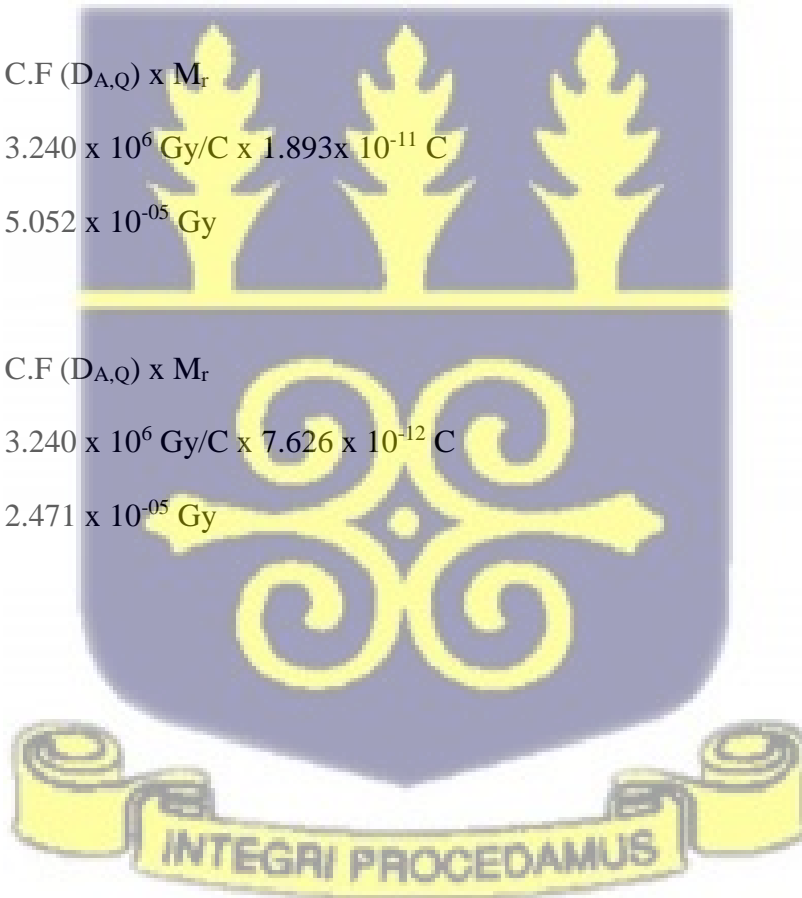
$$\begin{aligned}
 S_k (\text{Gycm}^2\text{h}^{-1}) &= X_l \times l^2 \times (W/e) \\
 &= 3.191 \times 10^{-07} \text{ pCkg}^{-1}\text{s}^{-1}\text{m}^{-2} \times 0.002^2 \text{ m}^2 \times 33.97 \text{ kgC}^{-1} \\
 &= 4.336 \times 10^{-11} \text{ Gycm}^2\text{h}^{-1}
 \end{aligned}$$

*Dose distribution calculation*

$$\begin{aligned}
 \text{Dose (Gy)} &= \text{C.F (D}_{A,Q}) \times M_r \quad (4) \\
 &= 3.240 \times 10^6 \text{ Gy/C} \times 1.559 \times 10^{-11} \text{ C} \\
 &= 5.052 \times 10^{-05} \text{ Gy}
 \end{aligned}$$

$$\begin{aligned}
 \text{Dose (Gy)} &= \text{C.F (D}_{A,Q}) \times M_r \\
 &= 3.240 \times 10^6 \text{ Gy/C} \times 1.893 \times 10^{-11} \text{ C} \\
 &= 5.052 \times 10^{-05} \text{ Gy}
 \end{aligned}$$

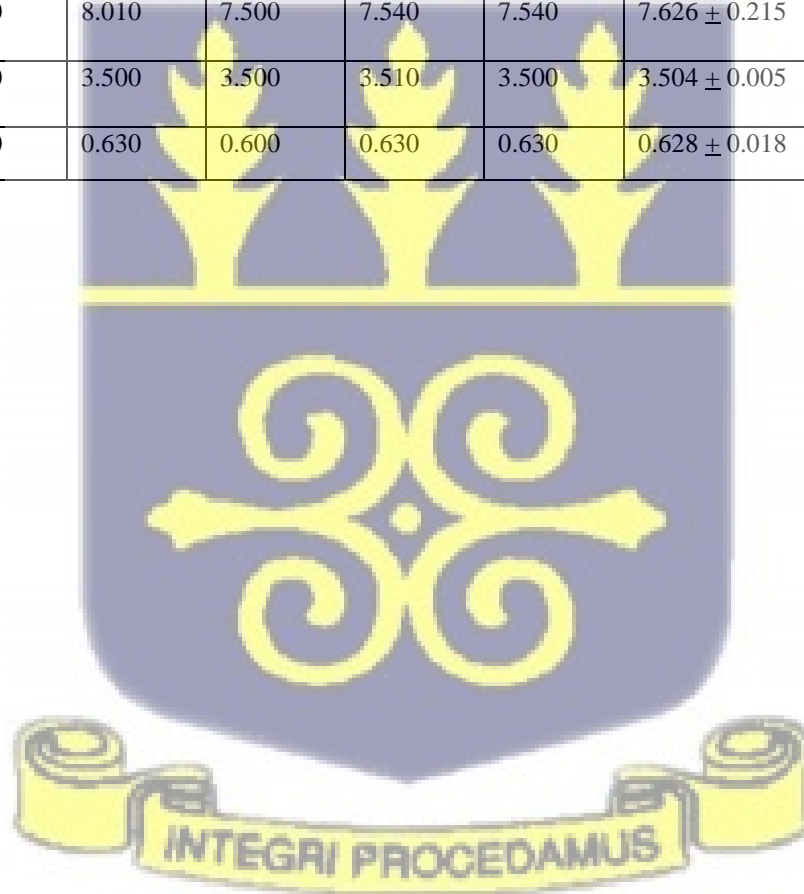
$$\begin{aligned}
 \text{Dose (Gy)} &= \text{C.F (D}_{A,Q}) \times M_r \\
 &= 3.240 \times 10^6 \text{ Gy/C} \times 7.626 \times 10^{-12} \text{ C} \\
 &= 2.471 \times 10^{-05} \text{ Gy}
 \end{aligned}$$



**7.1 Appendix 2: Dose distribution in water phantom**

Table 4. Charge values of dose distribution with varying distances at the right side of the source.

Direction of Exposure	Distance (cm)	Charge (pC)					Average (pC)	Dose (Gy)
Right	2	15.700	15.200	15.660	15.700	15.700	15.592 ± 0.220	5.052 x 10 <sup>-5</sup>
	5	2.530	2.450	2.450	2.450	2.450	2.466 ± 0.036	7.990 x 10 <sup>-6</sup>
	7	0.310	0.340	0.310	0.350	0.330	0.328 ± 0.018	1.063 x 10 <sup>-6</sup>
Left	2	18.950	18.920	18.920	18.910	18.950	18.930 ± 0.019	6.133 x 10 <sup>-5</sup>
	5	4.120	4.330	4.330	4.330	4.330	4.288 ± 0.094	1.389 x 10 <sup>-5</sup>
	7	0.310	0.340	0.310	0.350	0.330	0.328 ± 0.018	1.063 x 10 <sup>-6</sup>
Top	2	7.540	8.010	7.500	7.540	7.540	7.626 ± 0.215	2.471 x 10 <sup>-5</sup>
	5	3.510	3.500	3.500	3.510	3.500	3.504 ± 0.005	1.13 x 10 <sup>-5</sup>
	7	0.650	0.630	0.600	0.630	0.630	0.628 ± 0.018	2.035 x 10 <sup>-6</sup>



**7.1 Appendix 3: Cross calibration**

Radiation Quantity Measurement on Cobalt.

1. A19

$T_{IN} - 24^{\circ}C$

$T_{FIN} - 22.6^{\circ}C$

$P_{IN} - 98.4hPa$

$P_{FIN} - 98.5hPa$

Table 5. Charge values of radiation quantity at a depth of 10cm in phantom.

A19						
Voltage	Charge (nC)					Average (nC)
+ 300V	-5.820	-5.820	-5.830	-5.830	-5.840	$-5.828 \pm 0.006$
-300V	5.530	5.530	5.530	5.540	5.540	$5.534 \pm 0.000$
+ 100V	-5.840	-5.830	-5.850	-5.830	-5.850	$5.840 \pm 0.01$
PTW 31010						
+ 300V	-0.900	-0.900	-0.900	-0.900	-0.901	$-0.900 \pm 0.000$
-300V	0.900	0.900	0.899	0.737	0.899	$0.867 \pm 0.073$
+ 100V	-0.895	-0.895	-0.896	-0.896	-0.896	$-0.896 \pm 0.000$



Ionization Recombination Measurement on Cobalt (TPR<sub>10, 20</sub>).

1. A19

T<sub>IN</sub> : 24.6<sup>0</sup>C

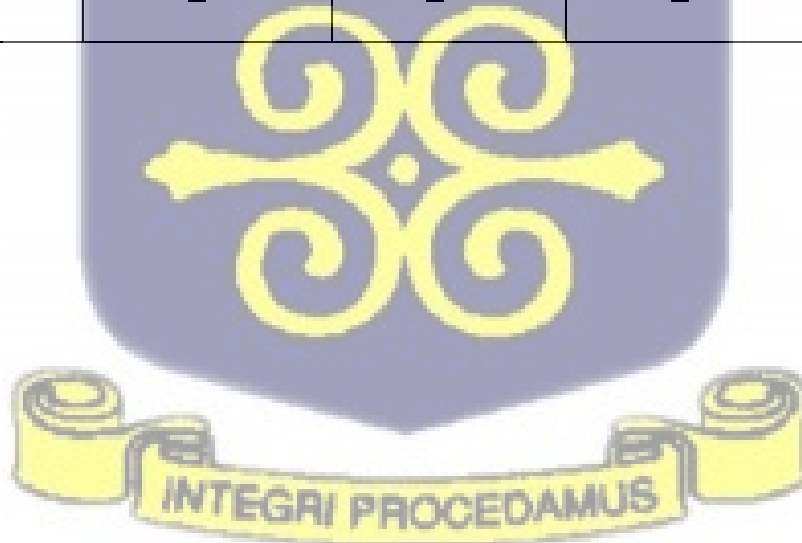
T<sub>FIN</sub> : 24.0<sup>0</sup>C

P<sub>IN</sub> : 98.9hPa

P<sub>FIN</sub> : 98.8hPa

Table 6. Charge values of ionization recombination measurement at a depth of 10cm in phantom.

Depth	10 (cm)		20 (cm)	
	+300V	-300V	+300V	-300V
Charge (nC)	-5.830	5.460	-3.450	3.000
	-5.800	5.330	-3.550	3.010
	-5.800	5.460	-3.550	3.030
	-5.850	5.460	-3.550	3.010
	-5.850	5.460	-3.550	3.010
Average	-5.826 ± 0.025	5.434 ± 0.058	-3.530 ± 0.045	3.012 ± 0.011



2. PTW 31010

Table 7. Charge values of ionization recombination measurement at a depth of 10cm in phantom.

Depth	10 (cm)		20 (cm)	
	+300V	-300V	+300V	-300V
Charge (nC)	-0.657	0.668	-0.504	0.435
	-0.658	0.665	-0.505	0.436
	-0.658	0.670	-0.505	0.435
	-0.659	0.670	-0.505	0.434
	-0.658	0.670	-0.503	0.435
Average (nC)	$-0.658 \pm 0.000$	$0.669 \pm 0.003$	$-0.504 \pm 0.001$	$0.435 \pm 0.001$



Ionization Recombination Measurement on LINAC.

1. A19

$T_{IN} : 20.5^{\circ}C$

$T_{FIN} : 20.5^{\circ}C$

$P_{IN} : 98.6hPa$

$P_{FIN} : 98.6hPa$

Table 8. Charge values of ionization recombination measurement at a depth of 10cm in phantom.

A19						
Depth	10 (cm)			20 (cm)		
Voltage	+300V	-300V	+100V	+300V	-300V	+100V
Charge (nC)	-16.710	16.760	-16.640	-10.970	10.930	-10.880
	-16.720	16.750	-16.670	-10.930	10.960	-10.960
	-16.730	16.740	-16.630	-10.950	10.920	-10.920
	-16.700	16.760	-16.620	-10.980	10.920	-10.920
	-16.700	16.740	-16.600	-10.920	10.930	-10.930
Average (nC)	-16.712±0.013	16.750±0.010	-16.632±0.026	-10.950±0.025	10.932±0.016	-10.9220±0.029
PTW 31010						
Charge (nC)	-2.633	2.765	-2.619	-1.818	1.711	-1.691
	-2.634	2.762	-2.620	-1.814	1.695	-1.696
	-2.635	2.767	-2.619	-1.817	1.701	-1.696
	-2.639	2.766	-2.619	-1.813	1.701	-1.694
	-2.630	2.763	-2.617	-1.813	1.701	-1.696
Average (nC)	-2.634±0.003	2.765±0.002	-2.619±0.001	-1.815±0.002	1.702±0.006	-1.695±0.002

*Cross calibration calculations*

$$C.F. = \frac{M_s}{M_r} \times K_{Q,Q_0} \times N_A \quad (5)$$

Where,

$M_s$  – Charge values of standard ion chamber reading from the electrometer

$M_r$  – uncorrected charge values from reference ion chamber reading from the electrometer

$I_s$  – Charge values of ionization recombination values of the standard ion chamber

$I_r$  – Charge values of ionization recombination values of the reference ion chamber

$N_A$  – Nominal dose of standard ion chamber

**Cobalt**

$$K_{T,P} = \left( \frac{273.2 + T}{273.2 + T_0} \right) \frac{P}{P_0} \quad (6)$$

$$K_{T,P} = \left( \frac{273.2 + 24.6^{\circ}C}{273.2 + 24.0^{\circ}C} \right) \times \frac{98.5hPa}{98.4hPa}$$

$$K_{T,P} = 1.030$$

**Linac**

$$K_{T,P} = \left( \frac{273.2 + T}{273.2 + T_0} \right) \frac{P}{P_0}$$

$$K_{T,P} = \left( \frac{273.2 + 20.5^{\circ}C}{273.2 + 20.5^{\circ}C} \right) \times \frac{98.6hPa}{98.6hPa}$$

$$K_{T,P} = 1.000$$

$$K_{POL} = \frac{|M_+| + |M_-|}{2M} \quad (7)$$

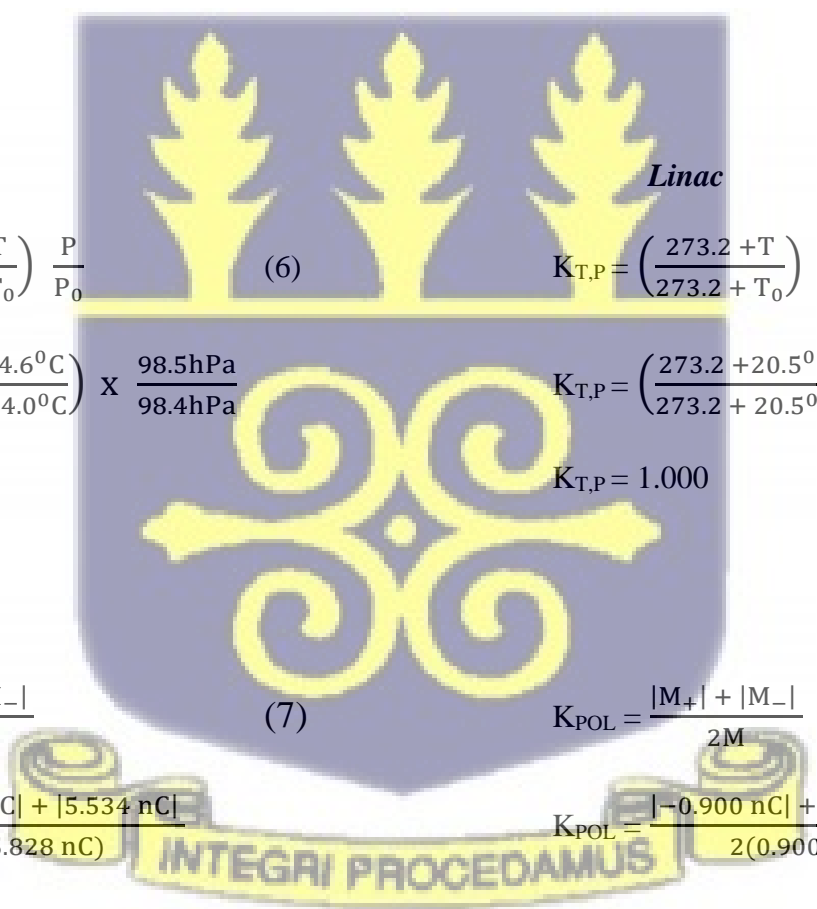
$$K_{POL} = \frac{|-5.828 \text{ nC}| + |5.534 \text{ nC}|}{2(5.828 \text{ nC})}$$

$$K_{POL} = 0.975$$

$$K_{POL} = \frac{|M_+| + |M_-|}{2M}$$

$$K_{POL} = \frac{|-0.900 \text{ nC}| + |0.867 \text{ nC}|}{2(0.900 \text{ nC})}$$

$$K_{POL} = 0.982$$



$$K_S = \frac{I_S}{I_R} \quad (8)$$

$$K_S = \frac{I_S}{I_R}$$

$$K_S = \frac{-5.826 \text{ nC}}{-0.658 \text{ nC}}$$

$$K_S = \frac{-16.712 \text{ nC}}{-0.2.634 \text{ nC}}$$

$$K_S = 8.854$$

$$K_S = 6.345$$

$$QI (K_{Q,Q_0}) = K_S K_{POL} K_{T,P}$$

$$QI (K_{Q,Q_0}) = K_S K_{POL} K_{T,P}$$

$$QI (K_{Q,Q_0}) = 1.030 \times 0.975 \times 8.85$$

$$QI (K_{Q,Q_0}) = 1.000 \times 0.982 \times 6.345$$

$$QI (K_{Q,Q_0}) = 8.892$$

$$QI (K_{Q,Q_0}) = 6.231$$

$$C.F = \frac{M_S}{M_r} \times K_{Q,Q_0} \times N_D$$

$$= \frac{-5.828}{-0.900} \times 8.892 \times 4.771 \times 10^7 \text{ Gy/C}$$

$$= 3.240 \times 10^6 \text{ Gy/C}$$

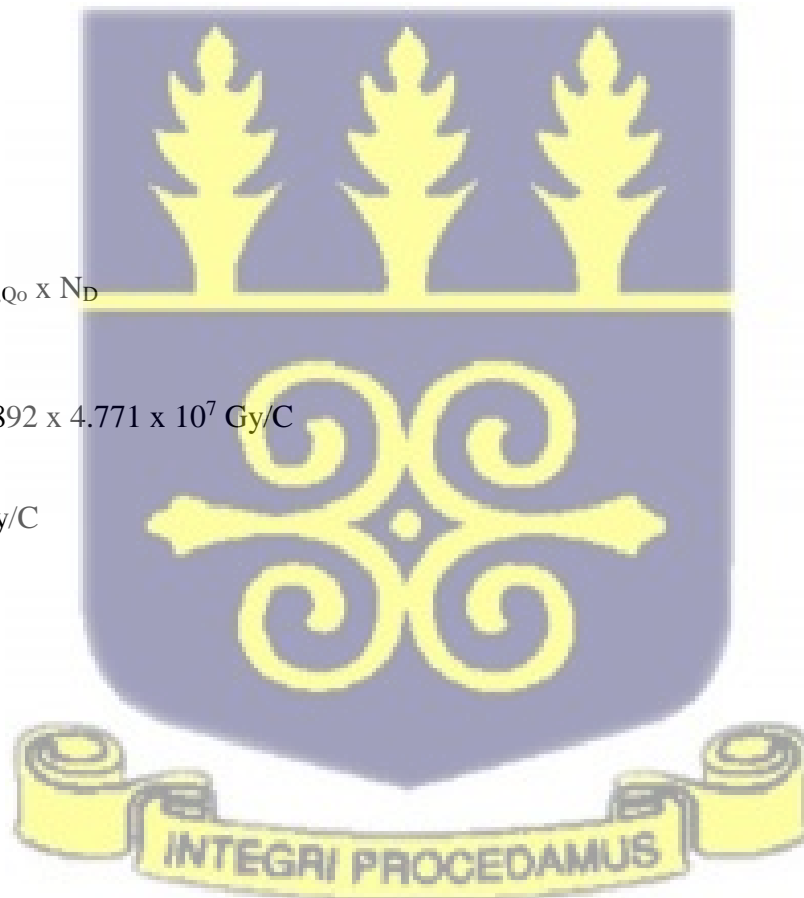


Table 9. Parameters for correction factor calculation for cross calibration

Bias Voltage: + 300V

Nominal Beam Energy	Cobalt		6MV	
Depth	10 cm	20 cm	10 cm	20 cm
$I_s$	-5.826 nC	-3.530 nC	-16.712 nC	-10.950 nC
$I_F$	-0.658 nC	-0.504 nC	-2.634 nC	-1.815 nC
$K_{T,P}$	1.030		1.000	
$K_s$	8.854		6.216	
$K_{pol}$	0.975		0.982	
QI ( $K_{Q,Q0}$ )	8.892		6.231	
$N_A$ (cGy/nC)	$4.771 \times 10^7$ Gy/C			
$\frac{M_S}{M_F}$ (nC/div)	6.476		6.345	
CF(Gy/C)	$3.240 \times 10^6$ Gy/C $\pm$ 0.06			

